



# Exclusive neuronal detection of KGDHC-specific subunits in the adult human brain cortex despite pancellular protein lysine succinylation

Arpad Dobolyi<sup>1,2</sup> · Attila Bago<sup>3</sup> · Miklos Palkovits<sup>1</sup> · Natalia S. Nemeria<sup>4</sup> · Frank Jordan<sup>4</sup> · Judit Doczi<sup>5</sup> · Attila Ambrus<sup>5,6</sup> · Vera Adam-Vizi<sup>5,6</sup> · Christos Chinopoulos<sup>5</sup> 

Received: 6 January 2019 / Accepted: 11 January 2020 / Published online: 25 January 2020  
© The Author(s) 2020

## Abstract

The ketoglutarate dehydrogenase complex (KGDHC) consists of three different subunits encoded by *OGDH* (or *OGDHL*), *DLST*, and *DLD*, combined in different stoichiometries. *DLD* subunit is shared between KGDHC and pyruvate dehydrogenase complex, branched-chain alpha-keto acid dehydrogenase complex, and the glycine cleavage system. Despite KGDHC's implication in neurodegenerative diseases, cell-specific localization of its subunits in the adult human brain has never been investigated. Here, we show that immunoreactivity of all known isoforms of *OGDHL*, *OGDH*, and *DLST* was detected exclusively in neurons of surgical human cortical tissue samples identified by their morphology and visualized by double labeling with fluorescent Nissl, while being absent from glia expressing GFAP, Aldh11, myelin basic protein, Olig2, or IBA1. In contrast, *DLD* immunoreactivity was evident in both neurons and glia. Specificity of anti-KGDHC subunits antisera was verified by a decrease in staining of siRNA-treated human cancer cell lines directed against the respective coding gene products; furthermore, immunoreactivity of KGDHC subunits in human fibroblasts co-localized > 99% with mitotracker orange, while western blotting of 63 post-mortem brain samples and purified recombinant proteins afforded further assurance regarding antisera monospecificity. KGDHC subunit immunoreactivity correlated with data from the Human Protein Atlas as well as RNA-Seq data from the Allen Brain Atlas corresponding to genes coding for KGDHC components. Protein lysine succinylation, however, was immunohistochemically evident in all cortical cells; this was unexpected, because this posttranslational modification requires succinyl-CoA, the product of KGDHC. In view of the fact that glia of the human brain cortex lack succinate-CoA ligase, an enzyme producing succinyl-CoA when operating in reverse, protein lysine succinylation in these cells must exclusively rely on propionate and/or ketone body metabolism or some other yet to be discovered pathway encompassing succinyl-CoA.

**Keywords** Mitochondria · Succinyl-CoA · Citric acid cycle · Ketoglutarate dehydrogenase

**Electronic supplementary material** The online version of this article (<https://doi.org/10.1007/s00429-020-02026-5>) contains supplementary material, which is available to authorized users.

✉ Christos Chinopoulos  
chinopoulos.christos@eok.sote.hu

<sup>1</sup> MTA-ELTE Laboratory of Molecular and Systems Neurobiology, Department of Physiology and Neurobiology, Hungarian Academy of Sciences and Eotvos Lorand University, Budapest 1117, Hungary

<sup>2</sup> Department of Anatomy, Histology and Embryology, Semmelweis University, Budapest 1094, Hungary

## Introduction

Ketoglutarate dehydrogenase complex (KGDHC) is a multi-subunit enzyme residing in the mitochondrial matrix (Maas and Bisswanger 1990). It catalyzes the irreversible decarboxylation of  $\alpha$ -ketoglutarate ( $\alpha$ Kg) to succinyl-CoA

<sup>3</sup> National Institute of Neurosurgery, Budapest 1145, Hungary

<sup>4</sup> Department of Chemistry, Rutgers University, Newark, NJ 07102-1811, USA

<sup>5</sup> Department of Medical Biochemistry, Semmelweis University, Tuzolto st. 37-47, Budapest 1094, Hungary

<sup>6</sup> MTA-SE Laboratory for Neurobiochemistry, Semmelweis University, Budapest 1094, Hungary

while reducing  $\text{NAD}^+$  to  $\text{NADH}$ . The complex participates in the citric acid cycle exhibiting a high flux-control coefficient in the generation of reducing equivalents (Cooney et al. 1981; Sheu and Blass 1999), also contributing to the maintenance of the mitochondrial redox state (Gibson et al. 2000). KGDHC's influence in the cycle is so significant; its activity dictates the directionality of all three of its segments (Chinopoulos 2013). KGDHC is further involved in transaminations and glutamate metabolism (Cooper 2012), while its product, succinyl-CoA, can be shuttled towards heme synthesis (Atamna et al. 2001; Atamna and Frey 2004; Burch et al. 2018), and/or mitochondrial substrate-level phosphorylation (mSLP). mSLP is almost exclusively attributed to succinyl-CoA ligase (SUCL), the enzyme following KGDHC in the citric acid cycle, catalyzing the reversible conversion of succinyl-CoA and ADP (or GDP) to CoASH, succinate, and ATP (or GTP) (Johnson et al. 1998). Unimpaired KGDHC activity is critical for sustaining mSLP (Kiss et al. 2013). Regulation of the complex and its overall impact on energy metabolism has been extensively reviewed elsewhere (Gibson et al. 2010; Starkov 2013).

More recently, the group of Gibson discovered that KGDHC serves as a trans-succinylase, adding succinyl moieties to lysines of proteins in an  $\alpha\text{K}_g$ -dependent manner (Gibson et al. 2015). Lysine succinylation is a widespread posttranslational modification occurring on thousands of lysines residing in hundreds of proteins distributed in the cytosol, nucleus, and mitochondria (Zhang et al. 2011; Weinert et al. 2013).

Mindful of KGDHC's involvement in a multitude of biochemical processes, it is not surprising that its deficiency leads to pathology, particularly in the brain: indeed, a decline in KGDHC activity is associated with Alzheimer's disease (Gibson et al. 1988, 1998, 2000, 2013; Butterworth and Besnard 1990; Mastrogiacoma et al. 1996; Terwel et al. 1998; Bubber et al. 2005), Parkinson's disease (Gibson et al. 2003), Huntington's chorea (Naseri et al. 2015), Wernicke–Korsakoff syndrome (Butterworth et al. 1993), and progressive supranuclear palsy (Albers et al. 2000; Park et al. 2001). A reduction of KGDHC activity is not generally paralleled by all other enzymes of the citric acid cycle (Bubber et al. 2005; Gibson et al. 2010; Bubber et al. 2011). The reason for this selective vulnerability is incompletely understood, but it is

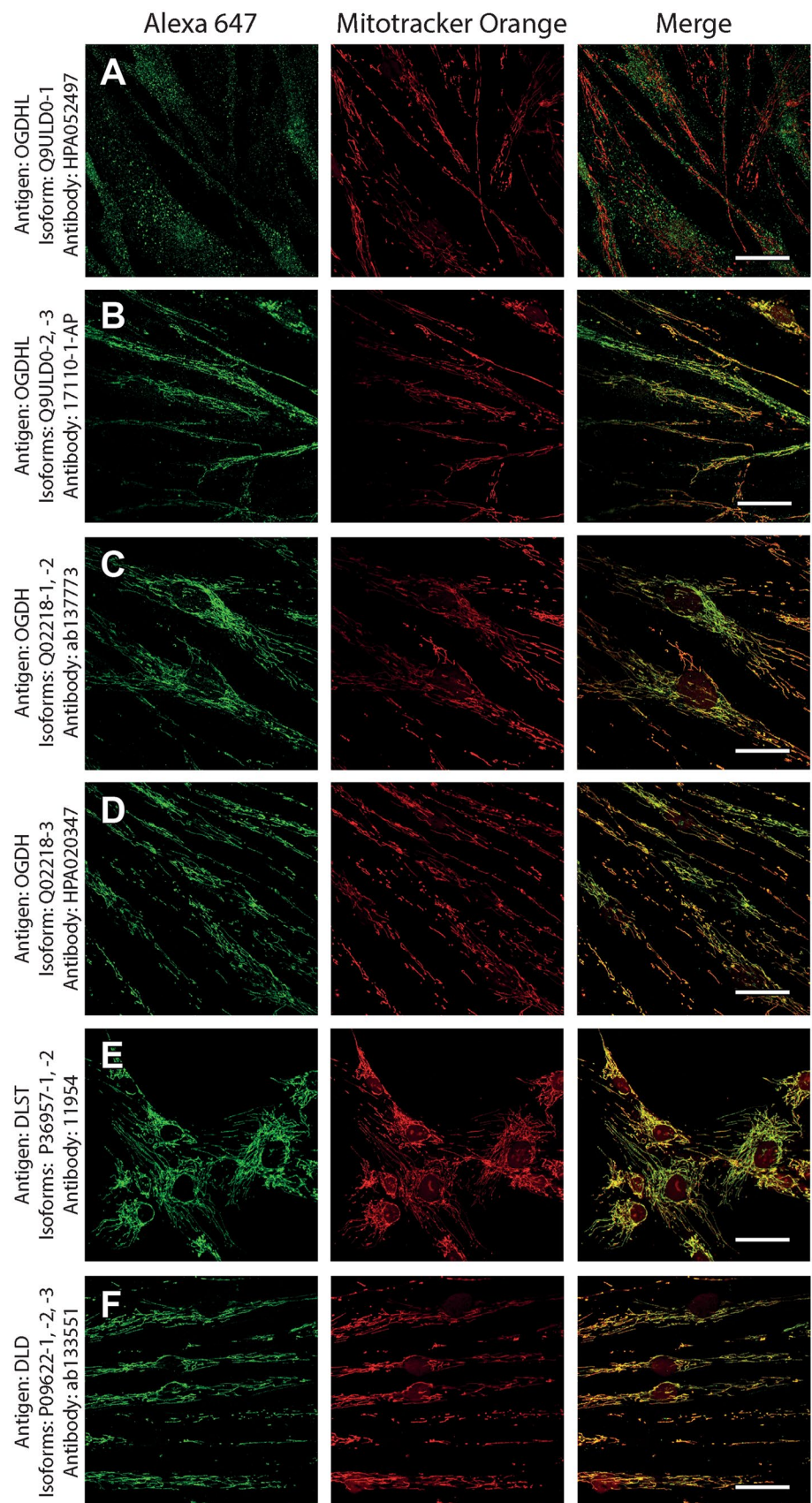
**Table 1** Antibodies used for detecting all known human KGDHC subunit isoforms

Subunit	Isoform	Antibody used
OGDHL	Q9ULD0-1	Atlas Antibodies, Cat# HPA052497, RRID:AB_2681853
	Q9ULD0-2	Proteintech Group, Cat# 17110-1-AP, RRID:AB_2156767
	Q9ULD0-3	Proteintech Group, Cat# 17110-1-AP, RRID:AB_2156767
OGDH	Q02218-1	Proteintech Group, Cat# 15212-1-AP, RRID:AB_2156759
	Q02218-2	Proteintech Group, Cat# 15212-1-AP, RRID:AB_2156759
	Q02218-3	Atlas Antibodies, Cat# HPA020347, RRID:AB_1854773
DLST	P36957-1	Cell Signaling Technology, Cat# 11954, RRID:AB_2732907
	P36957-2	Cell Signaling Technology, Cat# 11954, RRID:AB_2732907
DLG	P09622-1	Abcam, Cat# ab133551, RRID:AB_2732908
	P09622-2	Abcam, Cat# ab133551, RRID:AB_2732908
	P09622-3	Abcam, Cat# ab133551, RRID:AB_2732908

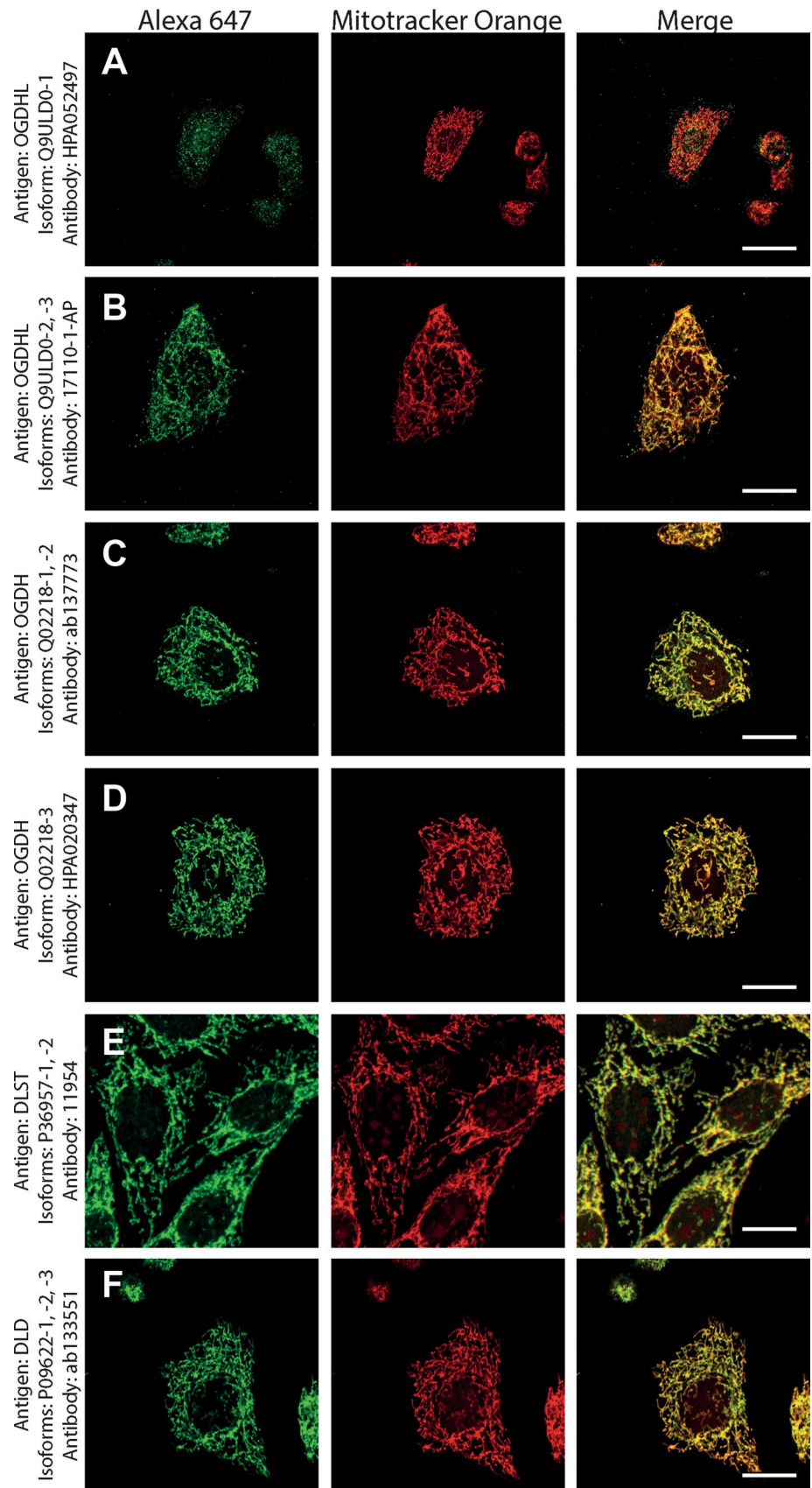
**Table 2** Antibodies directed against other targets used in this study

Target	Antibody used
GFAP	Santa Cruz Biotech, Cat# sc-33673, RRID:AB_627673
Aldh1l1	Abcam, Cat# ab177463, RRID: AB_2811300
Myelin basic protein	Abcam, Cat# ab24567, RRID:AB_448144
Olig2	Abcam, Cat# ab109186, RRID: AB_10861310
IBA1	Abcam, Cat# ab107159, RRID:AB_10972670
Succinyl-lysine	NovoPro, Cat# 106768, RRID:AB_2732922
VDAC1	Abcam, Cat# ab154856, RRID:AB_2687466
SUCLG1	Abcam, Cat# ab97867, RRID:AB_10678848
SUCLG2	Atlas Antibodies, Cat# HPA046705, RRID:AB_2679762
SUCLA2	Proteintech Group, Cat# 12627-1-AP, RRID:AB_2271200
$\beta$ -actin	Abcam, Cat# ab6276, RRID:AB_2223210

**Fig. 1** The demonstration of mitochondrial localization of OGDHL, OGDH, DLST, and DLD in human fibroblasts using the antibodies indicated on the left. OGDHL (**a**, **b**), OGDH (**c**, **d**), DLST (**e**), and DLD (**f**) immunolabeling (labelling by Alexa 647) in human fibroblasts in relation to mitotracker orange (MTO). Scale bars = 30  $\mu$ m for **a** and **c**, and 50  $\mu$ m for **b**, **d–f**



**Fig. 2** The demonstration of mitochondrial localization of OGDHL, OGDH, DLST, and DLD in HeLa cells using the antibodies indicated on the left. OGDHL (a, b), OGDH (c, d), DLST (e), and DLD (f) immunolabeling (labelling by Alexa 647) in HeLa cells in relation to mitotracker orange (MTO). Scale bars = 30  $\mu$ m for a and 15  $\mu$ m for b–f





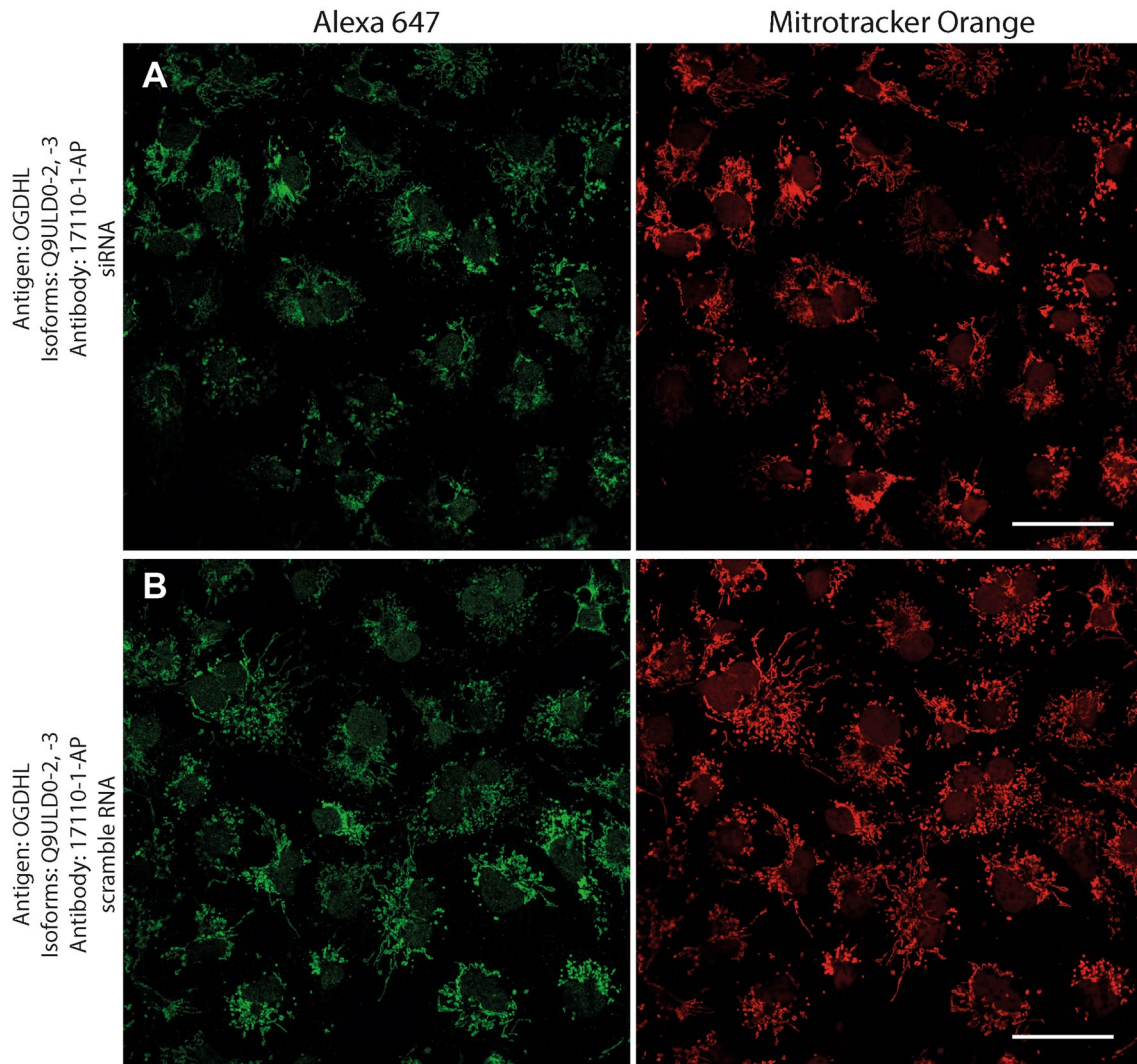


**Fig. 4** Effect of siRNA (a) vs scramble RNA (b) directed against OGDHL isoforms 2 and 3 on OGDHL immunostaining in COS-7 cells in relation to mitotracker orange (MTO). A reduced intensity

of OGDHL immunolabeling is visible following siRNA treatment as compared to scramble RNA treatment, while siRNA has no effect on the labeling with MTO. Scale bars = 50  $\mu$ m

## Materials and methods

### Human brains

Human brain samples were collected in accordance to the Ethical Rules for Using Human Tissues for Medical Research in Hungary (HM 34/1999) and the Code of Ethics of the World Medical Association (Declaration of Helsinki). Ethical permission for obtaining surgical brain material for the specific project has been obtained from the Medical Research Council of Hungary (No: 35302-5/2017/EKU), and is valid until June 30th, 2020. Post-mortem tissue samples were taken during brain autopsy in the framework of the Human Brain Tissue Bank (HBTB), Budapest, Hungary. HBTB has been authorized by the Committee

of Science and Research Ethic of the Ministry of Health of Hungary (No. 6008/8/2002/ETT) and the Semmelweis University Regional Committee of Science and Research Ethic (No. 32/1992/TUKEB). For autopsy, brains were removed from the skull with a post-mortem delay of 2–6 h. Prior written informed consent was obtained from the patients or from the next of kin for autopsies which included the request to conduct neurochemical analyses. The protocols including analyses of tissue samples were approved by institutional ethics committee of the Semmelweis University. The surgical patients (all males) underwent the removal of brain tumors; samples were obtained from normal brain cortical tissue removed during clearing the path for accessing the area of the tumor. All patients survived the surgery. The subjects whose brains were used

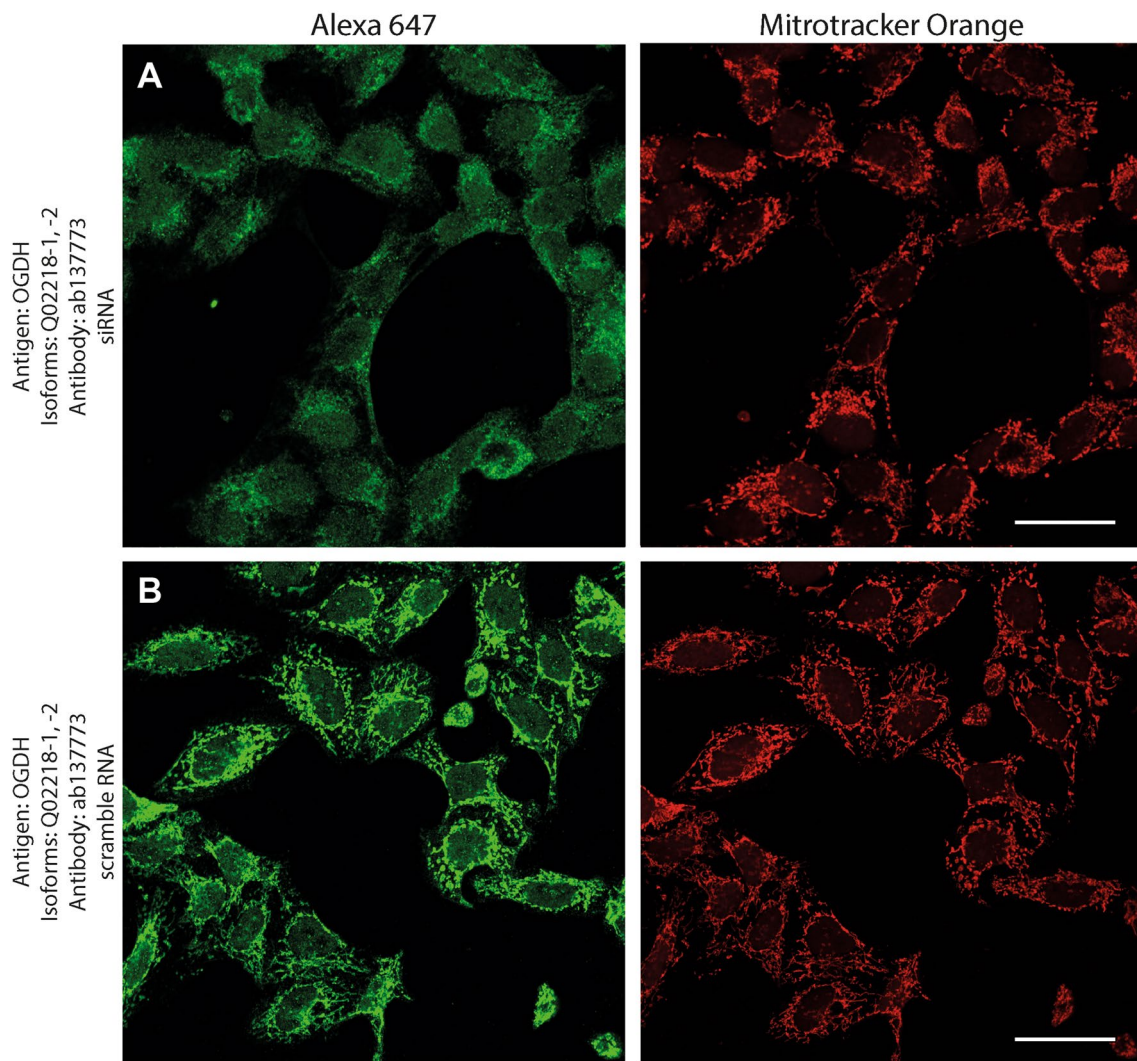


**Fig. 5** Effect of siRNA (a) vs scramble RNA (b) directed against OGDH isoforms 1 and 2 on OGDH immunostaining in HeLa cells in relation to mitotracker orange (MTO). A reduced intensity of OGDH

immunolabeling is visible following siRNA treatment as compared to scramble RNA treatment, while siRNA has no effect on the labeling with MTO. Scale bars = 50  $\mu$ m

in the autopsy study died without any known neurological or affective disorder. The medical history of the subjects was obtained from medical or hospital records, interviews with family members and relatives, as well as from pathological and neuropathological reports. All personal identifiers had been removed and samples were coded before the analyses of tissue. Surgical samples underwent immediate fixation (immersed in ice-cold 4% paraformaldehyde in 0.1 M phosphate-buffered saline within a few seconds after their excision from the brain) for immunolabeling used in histochemical techniques. For western blotting, autopsy samples from 63 different brain regions of 11 subjects (7 females and 4 males) were obtained by microdissection. Individual brain nuclei were microdissected from post-mortem brains (that have been rapidly frozen on dry ice and stored at  $-80^{\circ}\text{C}$ ) using the micropunch technique

(Palkovits 1973). Briefly, brains were cut as 1.0–1.5 mm-thick coronal sections, and individual brain regions and nuclei were removed by special punch needles with an inside diameter of 1.0–3.5 mm, using either a head magnifier or a stereomicroscope. The microdissected samples were collected in Eppendorf tubes and stored at  $-80^{\circ}\text{C}$  until further use. The temperature of brain sections and the microdissected samples was kept under  $0^{\circ}\text{C}$  during the whole procedure.

### Cell cultures

Fibroblast cultures from skin biopsies were prepared. Cells were grown on poly-L-ornithine coated 25 mm round glass coverslips for 5–7 days, at a density of approximately  $8 \times 10^5$  cells/coverslip in RPMI1640 medium (GIBCO, Life

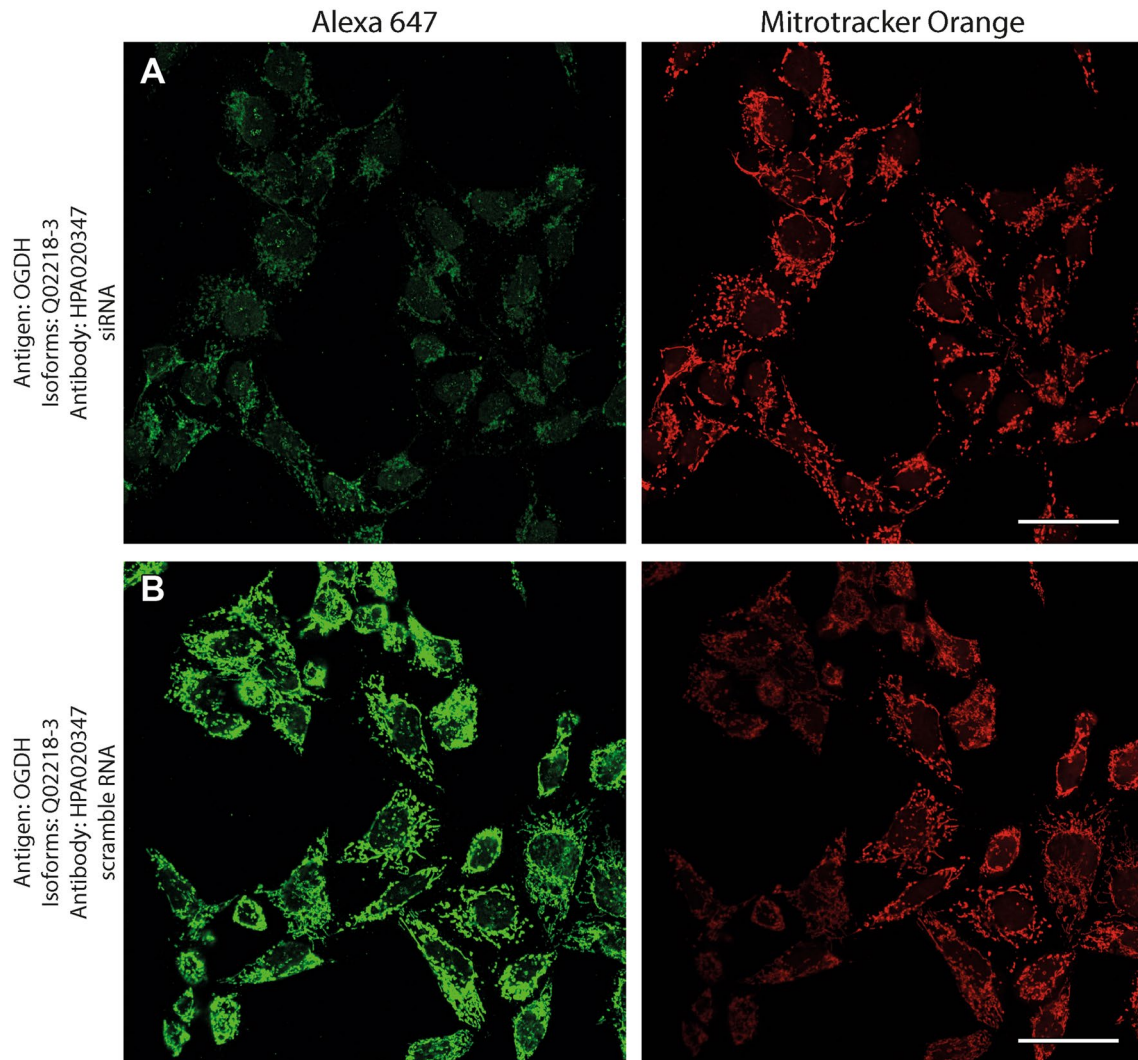


**Fig. 6** Effect of siRNA (a) vs scramble RNA (b) directed against OGDH isoform 3 on OGDH immunostaining in HeLa cells in relation to mitotracker orange (MTO). A reduced intensity of OGDH

immunolabeling is visible following siRNA treatment as compared to scramble RNA treatment, while siRNA has no effect on the labeling with MTO. Scale bars = 50  $\mu\text{m}$

technologies, Carlsbad, CA, USA) supplemented with 10% fetal bovine serum and 2 mM glutamine and kept at 37 °C in 5% CO<sub>2</sub>. The medium was also supplemented with penicillin, streptomycin, and amphotericin (item A5955, Sigma-Aldrich St. Louis, MO, USA). HeLa cells were grown on poly-L-ornithine coated 25 mm round glass coverslips for 1–2 days, at a density of approximately  $5 \times 10^5$  cells/coverslip in DMEM (GIBCO) plus glutamine plus 10% fetal calf serum and 1% streptomycin-penicillin.

### Tissue collection for immunolabeling

For immunocytochemistry, brains were cut into 5–10 mm-thick coronal slices and immersion-fixed in 4% paraformaldehyde in 0.1 M phosphate-buffered saline (PBS) for 3–5 days. Subsequently, the blocks were transferred to PBS

containing 0.1% sodium azide for 2 days to remove excess paraformaldehyde. Then, the blocks were placed in PBS containing 20% sucrose for 2 days for cryoprotection, after which the blocks were frozen and cut into 50  $\mu\text{m}$ -thick serial coronal sections on a sliding microtome. Sections were collected in PBS containing 0.1% sodium azide and stored at 4 °C until further processing.

### DAB immunolabeling of brain sections

Every fifth free-floating brain section of human temporal and frontal cortical blocks was immunostained for KGDHC subunits. First, the sections were rinsed in PBS containing 0.3% Triton X-100 and 1% bovine serum albumin (BSA) for 1 h to improve antibody penetration and reduce nonspecific labeling, respectively. Subsequently, the antibodies were

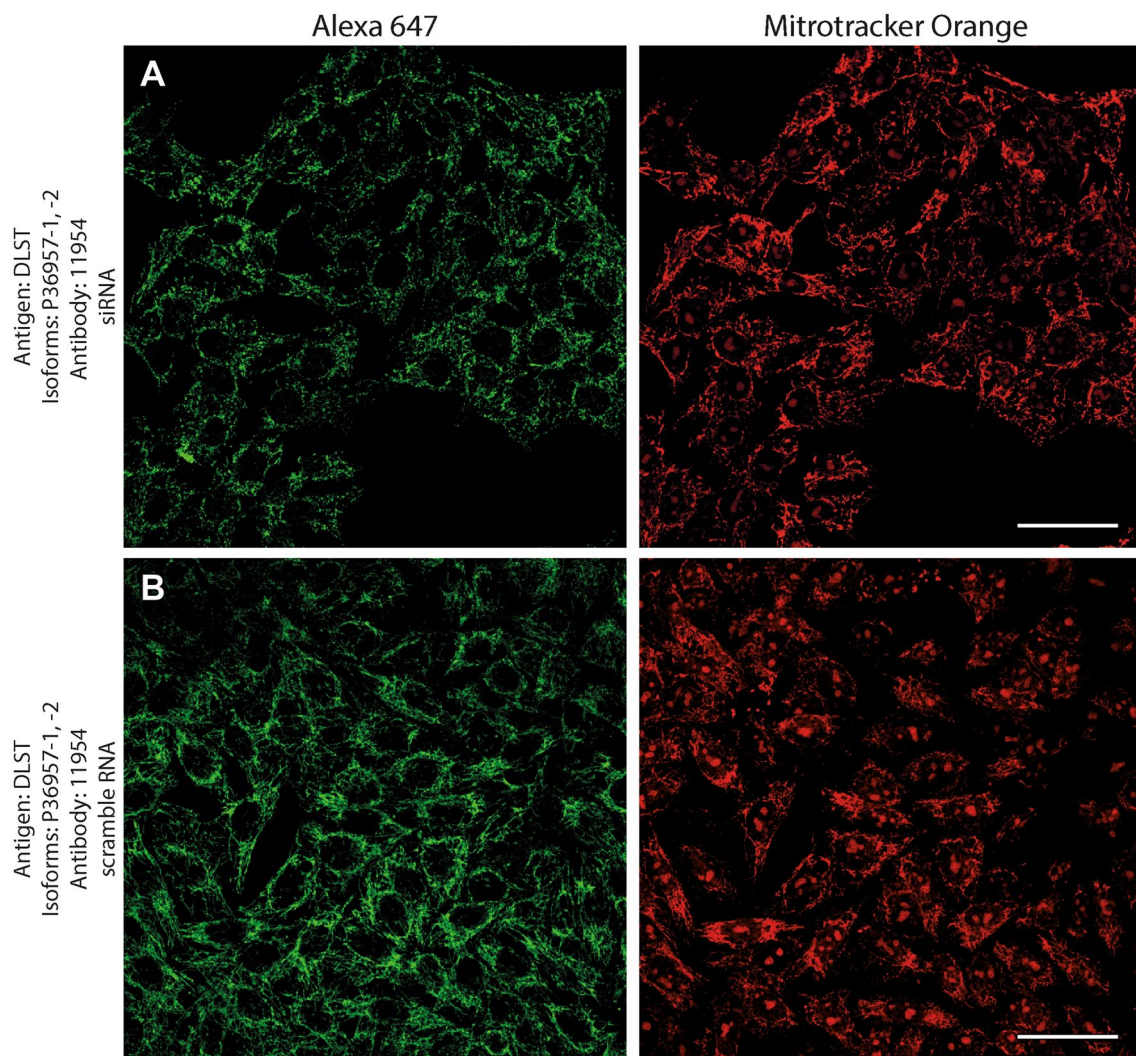


**Fig. 7** Effect of siRNA (a) vs scramble RNA (b) directed against DLST isoforms 1 and 2 on DLST immunostaining in HeLa cells in relation to mitotracker orange (MTO). A reduced intensity of DLST

immunolabeling is visible following siRNA treatment as compared to scramble RNA treatment, while siRNA has no effect on the labeling with MTO. Scale bars = 50  $\mu$ m

applied for 48 h at room temperature, followed by incubation of the sections in biotinylated anti-rabbit secondary antibody (1:1,000 dilution; Vector Laboratories, Burlingame, CA) and then in avidin–biotin–peroxidase complex (1:500; Vector Laboratories) for 2 h. Subsequently, the labeling was visualized by incubation in 0.02% 3,3-diaminobenzidine (DAB; Sigma), 0.08% nickel (II) sulfate, and 0.001% hydrogen peroxide in PBS, pH = 7.4 for 5 min. Sections were mounted, dehydrated, and coverslipped with Cytoseal 60 (Stephens Scientific, Riverdale, NJ, USA).

### Double labeling of in brains sections

KGDHC subunits were immunolabeled using fluorescein isothiocyanate (FITC)-tyramide amplification immunohistochemistry, which was followed by labeling neurons and

glial cells in a subsequent step. FITC-tyramide amplification immunolabeling of KGDHC subunits was performed as the single labeling except that visualization in the last step was done using fluorescein isothiocyanate (FITC)-tyramide (1:8,000) and  $H_2O_2$  in 100 mM Trizma buffer (pH 8.0 adjusted with HCl) applied for 6 min, instead of DAB. Subsequently, sections were placed in mouse anti-glial fibrillary acidic protein (GFAP), a marker of astrocytes (1:300, Santa Cruz Biotechnology, Delaware, CA, USA; see Table 2), rabbit anti-aldehyde dehydrogenase 1 family member L1 (Aldh1l1), a marker of astrocytes (1:50, Abcam, Cambridge, UK; see Table 2), rabbit anti-oligodendrocyte transcription factor 2 (Olig2), a marker of oligodendrocytes (1:50, Abcam, Cambridge, UK; see Table 2), mouse anti-myelin basic protein (MBP), a marker of oligodendrocytes (1:300, Abcam, Cambridge, UK; see Table 2), or goat

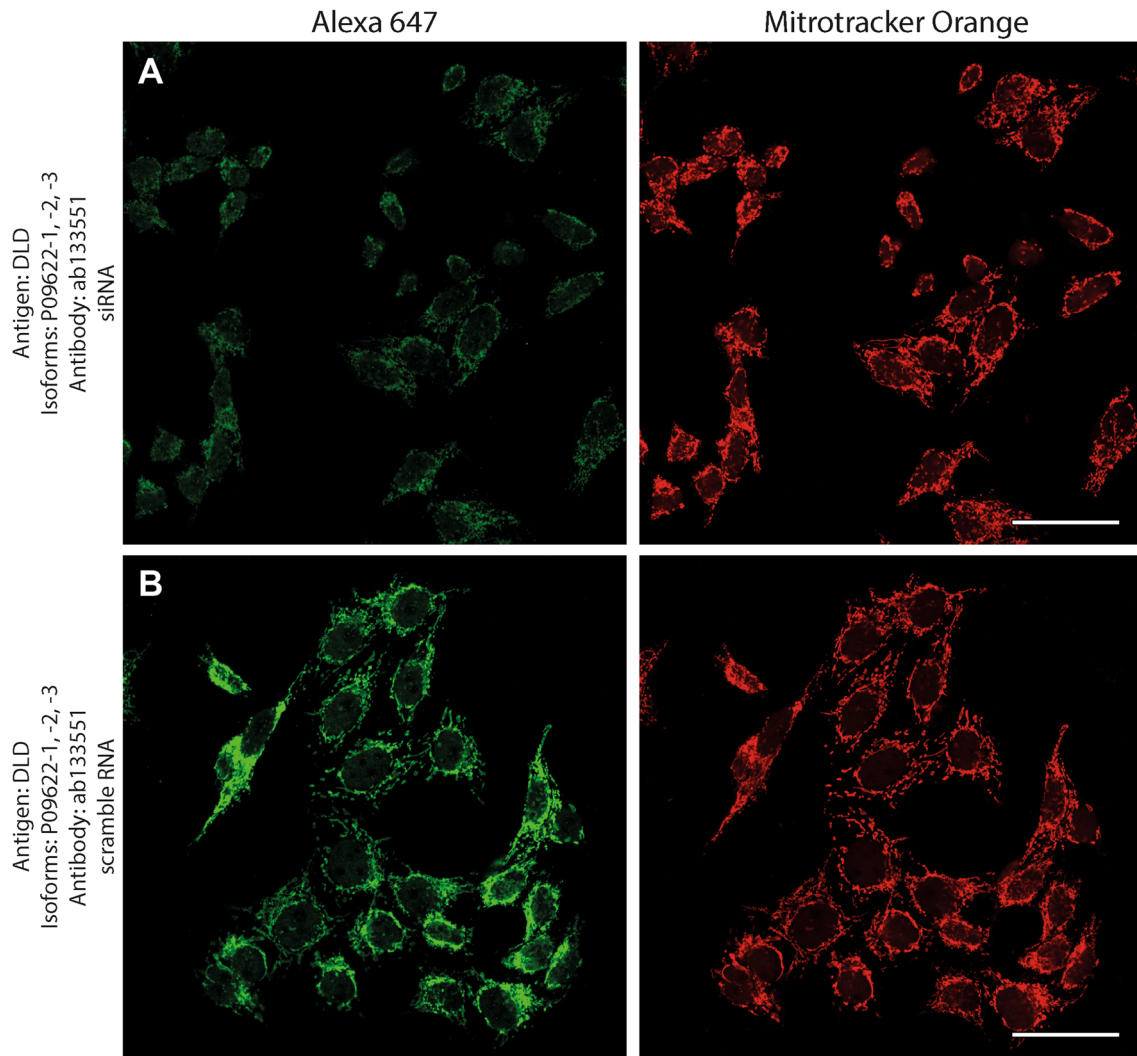


**Fig. 8** Effect of siRNA (a) vs scramble RNA (b) directed against DLD isoforms 1, 2 and 3 on DLD immunostaining in HeLa cells in relation to mitotracker orange (MTO). A reduced intensity of DLD

immunolabeling is visible following siRNA treatment as compared to scramble RNA treatment, while siRNA has no effect on the labeling with MTO. Scale bars = 50  $\mu$ m

anti-ionized calcium-binding adaptor molecule 1 (Iba1), a marker of microglial cells (1:1000, Abcam, Cambridge, UK; see Table 2) for 48 h at room temperature. The sections were then incubated in Alexa 594 donkey anti-mouse (or rabbit, or goat, respectively) secondary antibody (1:500, Molecular Probes, Eugene, OR) for 2 h and washed. For the double labeling with Nissl staining, the sections were incubated in ‘Neurotrace’ red fluorescent Nissl stain (Molecular Probes) diluted to 1:30 for 2 h, and washed in PBS overnight. Finally, all sections with fluorescent labels were mounted on positively charged slides (Superfrost Plus, Fisher Scientific, Pittsburgh, PA) and coverslipped in antifade medium (Prolong Antifade Kit, Molecular Probes).

### Immunocytochemistry of cell cultures

Fibroblasts or HeLa (CLS Cat# 300194/p772\_HeLa, RRID:CVCL\_0030) or COS-7 (CLS Cat# 605470/p532\_COS-7, RRID:CVCL\_0224) cell cultures were first treated with 1  $\mu$ M Mitotracker Orange (MTO) for 5 min in their culture media, at 37  $^{\circ}$ C in 5% CO<sub>2</sub>. Subsequent immunocytochemistry of the cultures was performed by fixing the cells with 4% paraformaldehyde in PBS for 20 min, followed by permeabilization by 0.1% TX-100 (in PBS) for 10 min and several washing steps in between with PBS at room temperature. Cultures were treated with 10% donkey serum overnight at 4  $^{\circ}$ C followed by bathing in 1% donkey serum and a primary antibody as indicated in Tables 1 and 2 for 12 h at room temperature. Titers are indicated in the respective legends. Cells were subsequently

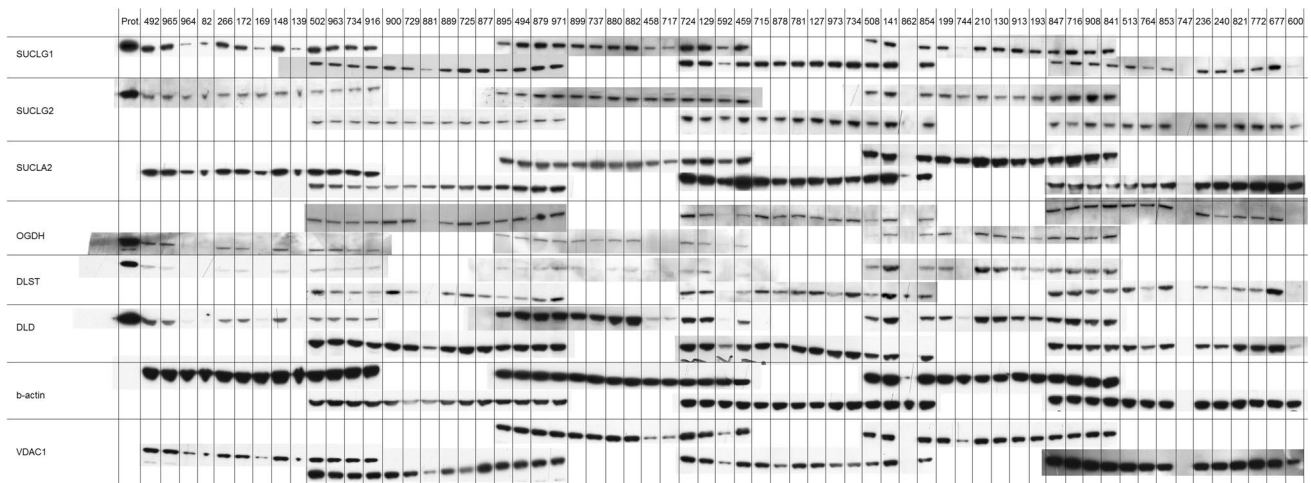


**Fig. 9** Immunoreactivities of the proteins indicated on the left in brain tissue homogenates (indicated on the top; individual samples coded by a three-digit number obtained from brain regions as detailed

in Table 3). The most-left lane includes purified, recombinant proteins (Prot.) for SUCLG1, SUCLG2, OGDH, DLST, and DLD

decorated using the appropriate Alexa 488-linked or Alexa 647-linked secondary antibody (1:4,000, donkey anti-rabbit, Jackson Immunochemicals Europe Ltd, Cambridgeshire, UK) in the presence of 1% donkey serum.

### Western blotting

Frozen brain samples were thawed on ice in the presence of radioimmunoprecipitation assay buffer and a protease cocktail inhibitor containing: 0.5 mM 4-(2-aminoethyl) benzenesulfonyl fluoride hydrochloride, 150 nM Aprotinin, 1  $\mu$ M E-64, 0.5 mM EDTA disodium, and 1  $\mu$ M Leupeptin, and homogenized with a Teflon pestle. The suspensions were centrifuged once at 10,000g for 10 min, and the proteins present in the supernatants were separated by sodium dodecyl sulfate—polyacrylamide gel electrophoresis (SDS-PAGE). Separated proteins were transferred to a methanol-activated polyvinylidene difluoride membrane. Immunoblotting was performed as recommended by the manufacturers of the antibodies, see Tables 1 and 2. Immunoreactivity was detected using the appropriate peroxidase-linked secondary antibody (1:4,000, donkey anti-mouse or anti-rabbit, Jackson Immunochemicals Europe Ltd, Cambridgeshire, UK) and enhanced chemiluminescence detection reagent (ECL system; Amersham Biosciences GE Healthcare Europe GmbH, Vienna, Austria).

### Image processing

The sections were examined using an Olympus BX60 light microscope equipped with bright-field, dark-field and fluorescence. Images were captured at 2048  $\times$  2048 pixel

resolution with an SPOT Xplorer digital CCD camera (Diagnostic Instruments, Sterling Heights, MI, USA) using a 4 $\times$  objective for dark-field images, and 4–40 $\times$  objectives for bright-field and fluorescent images. Fluorescent sections were also evaluated using a Bio-Rad 2100 Rainbow Confocal System (Bio-Rad Laboratories, Inc, CA, USA). The contrast and sharpness of the images were adjusted using the “levels” and “sharpness” commands in Adobe Photoshop CS 8.0. Full resolution was maintained until the photomicrographs were finally cropped at which point the images were adjusted to a resolution of 300 dpi.

### siRNA and cell transfections

The ON-TARGETplus SMARTpool containing four different siRNA sequences, all specific to human KGDHC-specific components (see under “Results”) and the corresponding non-targeting control (scrambled RNA), were designed by Thermo Scientific Dharmacon and synthesized by Sigma-Aldrich. HeLa cells were transfected with 100 nM of either siRNA or scrambled siRNA using Lipofectamine 2000 according to the manufacturer’s instructions, 48 h before immunocytochemistry.

**Table 3** Brain regions of origin of samples

Sample identifier	Brain region
492	Insular cortex
965	putamen
964	caudate nucleus
82	Parahippocampal cortex
266	Entorhinal cortex
172	Somatosensory cortex
169	Cerebral white matter
148	Insular cortex
139	Cerebral white matter
502	Temporal cortex
963	Insular cortex
734	Posterior cingulate cortex
916	Parahippocampal cortex
900	Somatosensory cortex
729	Parahippocampal cortex
881	Cerebral white matter
889	Somatomotor cortex
725	Insular cortex
877	Dorsomedial prefrontal cortex
895	Temporal cortex
494	Anterior cingulate cortex
879	Frontopolar cortex
971	Frontal cortex
899	Caudal cingulate cortex
737	Entorhinal cortex
880	Parahippocampal cortex
882	Frontal cortex
458	Cerebral white matter (frontal)
717	Cerebral white matter (frontal)
724	Temporal cortex
129	Somatomotor cortex
592	Cerebral white matter (frontal)
459	Frontal cortex
715	Frontal cortex
878	Ventrolateral prefrontal cortex
781	Posterior cingulate cortex
127	Somatosensory cortex
973	Temporal cortex
734	Posterior cingulate cortex
508	Posterior cingulate cortex
141	Cerebral white matter (frontal)
862	Posterior cingulate cortex
854	Entorhinal cortex
199	Anterior cingulate cortex
744	Cerebral white matter (frontal)
210	Temporal cortex
130	Temporal cortex
913	medial geniculate body
193	Frontal cortex
847	Anterior cingulate cortex

**Table 3** (continued)

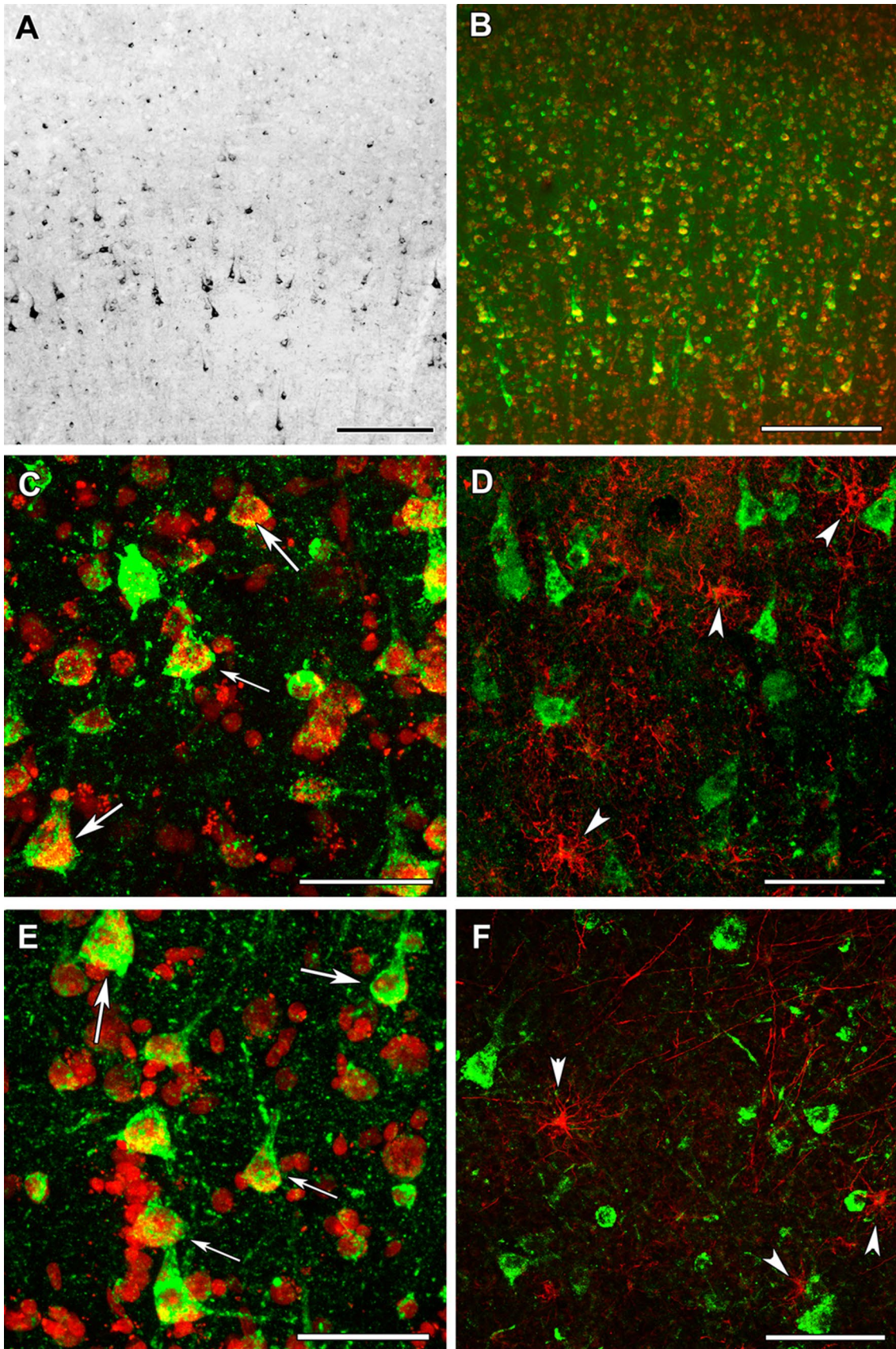
Sample identifier	Brain region
716	Anterior cingulate cortex
908	Frontal cortex
841	Insular cortex
513	Posterior cingulate cortex
764	Cerebral white matter (frontal)
853	Temporal cortex
747	Frontal cortex
236	Insular cortex
240	Parahippocampal cortex
821	Parahippocampal cortex
772	Temporal cortex
677	Entorhinal cortex
600	Cerebral white matter (frontal)

## Results

### Antibody selection for detecting all known KGDHC subunit human isoforms

KGDHC consists of multiple copies of three subunits: oxoglutarate dehydrogenase (OGDH) or oxoglutarate dehydrogenase-like protein (OGDHL), dihydrolipoyl succinyltransferase (DLST), and dihydrolipoyl dehydrogenase (DLD). OGDHL exhibits three isoforms Q9ULD0-1,

**Fig. 10** OGDHL immunolabeling in the human cerebral cortex in relation to neuronal and glial markers. **a** OGDHL isoform 1-immunoreactive cells are present in the cerebral cortex, with higher density in the deep layers. **b** OGDHL isoform 1 (green) and fluorescent Nissl staining (red) show many double-labeled yellow cells in the cerebral cortex. **c** A higher magnification confocal image of a cerebral cortical section double stained with OGDHL isoform 1 (green) and fluorescent Nissl staining (red) demonstrates that larger, neuronal cells (some of them indicated with white arrow) are double labeled. Several small cells are also present, which are not labeled with OGDHL isoform 1. Please observe the dot-like intracellular labeling pattern of OGDHL subunit 1 immunoreactivity. **d** A cerebral cortical section double labeled with OGDHL isoform 1 (green) and the established astrocyte marker glial fibrillary acidic protein (GFAP; red) shows only single-labeled cells positive for OGDHL isoform 1 or for GFAP, demonstrating that astrocytes are not labeled with OGDHL isoform 1. Some of the single-labeled astrocytes are pointed to by white arrowheads. **e** A confocal image of a cerebral cortical section double stained with OGDHL isoform 2/3 (green) and fluorescent Nissl staining (red) demonstrates that larger, neuronal cells (some of them indicated with white arrow) are double labeled. Several small cells not labeled with OGDHL isoform 2/3 are also present. Note the dot-like intracellular labeling pattern of OGDHL subunit 2/3 immunoreactivity. **f** A cerebral cortical section double labeled with OGDHL isoform 2/3 (green) and GFAP (red) shows cells labeled either with OGDHL or with GFAP, demonstrating that astrocytes are not labeled with OGDHL isoform 2/3. Some of the single-labeled astrocytes are pointed to by white arrowheads. Scale bars = 200  $\mu$ m for **a**, 300  $\mu$ m for **b**, 100  $\mu$ m for **c–f**



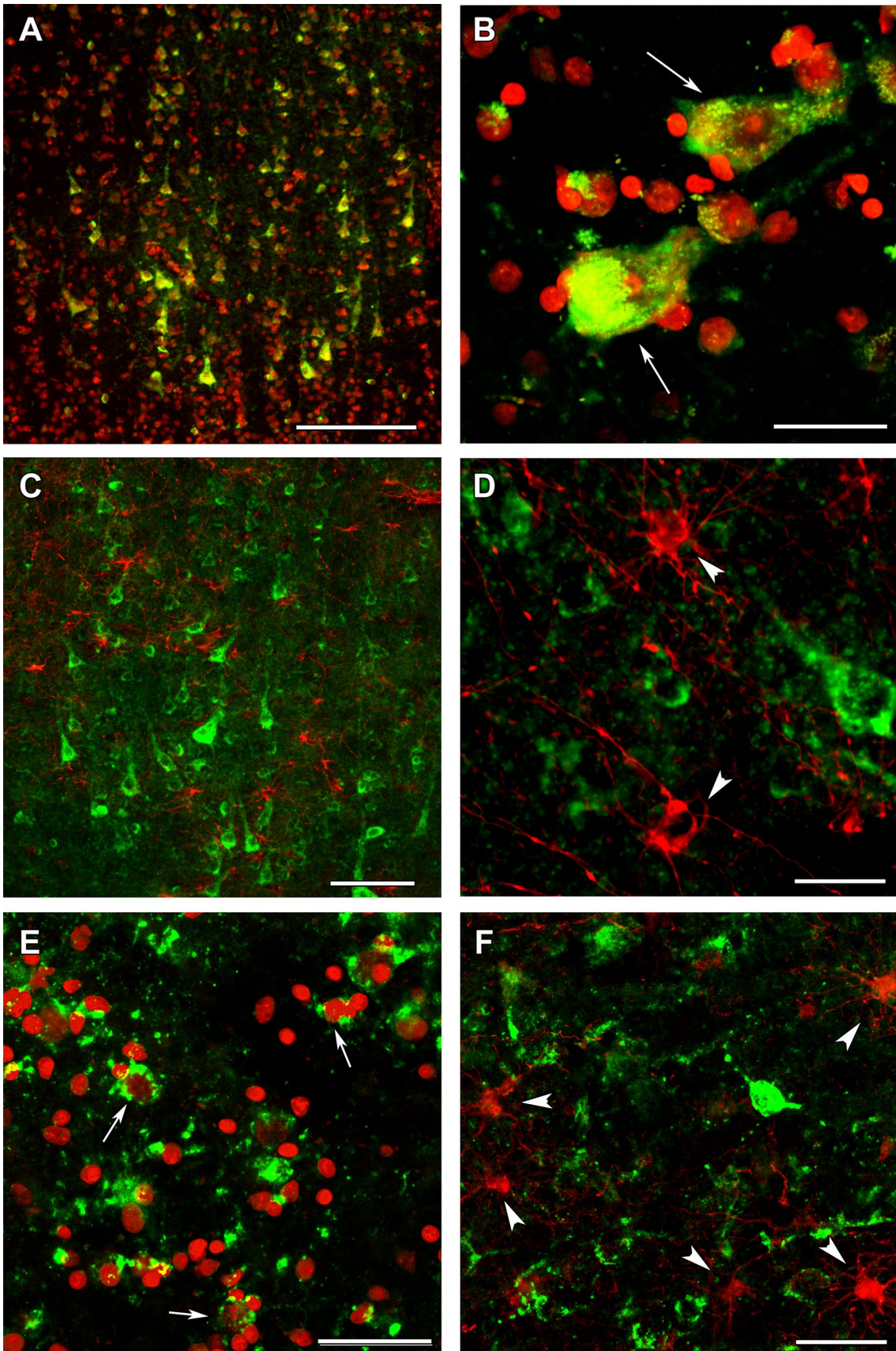


**Fig. 11** OGDH immunolabeling in the human cerebral cortex in relation to neuronal and glial markers. **a** OGDH isoform 1/2 (green) immunolabeling and fluorescent Nissl staining (red) show many double-labeled yellow cells in the cerebral cortex. **b** A high magnification confocal image of a cerebral cortical section double stained with OGDH isoform 1/2 (green) and fluorescent Nissl staining (red) demonstrates that larger, neuronal cells indicated with white arrow are double labeled. Several small cells are also present, which are not labeled with OGDH isoform 1/2. Note the dot-like intracellular labeling pattern of OGDH subunit 1/2 immunoreactivity. **c** A cerebral cortical section double labeled with OGDH isoform 1/2 (green) and the established astrocyte marker glial fibrillary acidic protein (GFAP; red) shows only single-labeled cells positive for OGDH isoform 1/2 or for GFAP, demonstrating that astrocytes are not labeled with OGDH isoform 1. **d** A high magnification confocal image shows separate single OGDH isoform 1/2 and GFAP-positive (red, pointed to by arrowheads) cells. **e** A confocal image of a cerebral cortical section double stained with OGDH isoform 3 (green) and fluorescent Nissl staining (red) demonstrates that larger, neuronal cells (some of them indicated with white arrow) are double labeled. Several small cells not labeled with OGDH isoform 3 are also present. **f** A cerebral cortical section double labeled with OGDH isoform 3 (green) and GFAP (red) shows cells labeled either with OGDH isoform 3 or with GFAP, demonstrating that astrocytes are not labeled with OGDH isoform 3. Some of the single-labeled astrocytes are pointed to by white arrowheads. Scale bars=200  $\mu\text{m}$  for **a**, 30  $\mu\text{m}$  for **b**, 100  $\mu\text{m}$  for **c**, 25  $\mu\text{m}$  for **d**, and 50  $\mu\text{m}$  for **e** and **f**

Q9ULD0-2 and Q9ULD0-3; OGDH 3 isoforms: Q02218-1, Q02218-2 and Q02218-3; DLST 2 isoforms: P36957-1 and P36957-2; and DLD 3 isoforms: P09622-1, P09622-2 and P09622-3. By knowing the amino acid sequence of each isoform, we could select antibodies raised using epitopes recognizing all isoforms, see Table 1. Whenever the same antibody is used for more than one isoform, this is because the epitope is within a 100% aligning region between the isoforms. More antibodies were probed that yielded no staining and these were excluded from this study.

### Antibody validation

Antibodies directed against KGDHC subunit isoforms were validated by the following protocols: (1) >99% co-localization with mitotracker orange (a dye that stains exclusively mitochondria) in human fibroblasts; (2) decrease in immunocytochemical staining of siRNA—but not scramble RNA-treated human cell lines silencing genes that code KGDHC subunit isoforms and decorated by the same antibodies; (3) emergence of only one band at the expected molecular weight in Western blots probing purified, recombinant proteins, and human brain homogenate samples.

As shown in Fig. 1, normal human fibroblasts were treated with the antibodies indicated on the left and detected with secondary antibodies conjugated with Alexa 647 fluorophore (left panels, green); their mitochondrial network was selectively stained by loading cells with Mitotracker Orange (MTO, 1  $\mu\text{M}$ , middle panels, red) prior to fixation.

Co-localization of Alexa 647 and MTO staining is shown in the panels to the right. From the right-hand panels, it is evident that except for antibody HPA052497 directed against isoform 1 of OGDHL (Q9ULD0-1), all other antibodies yielded >99% of co-localization with the mitochondrial network. Regarding Q9ULD0-1, at this junction, it cannot be distinguished if the lack of co-localization of the antibody with MTO is due to lack of specificity, or Q9ULD0-1 is not sufficiently expressed in human fibroblasts. Nonetheless, the robust co-localization of all other antibodies with MTO in these confocal images proved that the antigens are located within mitochondria.

Next, to investigate if the intramitochondrial decoration is due to antigens belonging to the intended proteins against which the KGDHC subunit and isoform-specific antibodies were raised, cell lines were transfected with either siRNA directed against individual subunits belonging to KGDHC or scramble RNA, and subsequently co-stained with the same antibodies and MTO. For these experiments, cancer cell lines (HeLa and COS-7) were used instead of fibroblasts, because the former exhibit much higher transfection efficiencies than the latter. COS-7 is a cell line originating from monkey kidney tissue, but it was probed for OGDHL isoforms 2 and 3 which are identical to those expressed in humans. Other cell lines tested did not yield a sufficiently clear mitochondrial network for co-localization studies (not shown). As shown in Fig. 2, HeLa cells were treated with the antibodies indicated on the left and decorated with secondary antibodies conjugated with Alexa 647 fluorophore (left panels, green); their mitochondrial network was selectively stained by loading cells with MTO (1  $\mu\text{M}$ , middle panels, red) prior to fixation. Co-localization of Alexa 647 and MTO staining is shown in the panels to the right. The robust co-localization of all antibodies (except HPA052497) with MTO in these confocal images proved that the antigens are located within mitochondria of HeLa cells as well. As shown in the top rows of Figs. 3, 4, 5, 6, 7, and 8, cells were treated with siRNA directed against the respective protein, and in the bottom rows with scramble RNA. Alexa 647 decoration is shown in panels to the left, while MTO staining is shown in the panels to the right. It is evident that the mitochondrial staining for KGDHC subunits shown in siRNA-treated cells (top-left images) appears weaker than the scramble RNA-treated cells (bottom-left panels); furthermore, in some instances (top left panels in Figs. 5, 6, and 8), the mitochondrial network of siRNA-treated cells is more fragmented than those treated with the scramble RNA. The decrease in staining together with the alterations in mitochondrial network in siRNA-treated but not scramble RNA-treated cells strongly argues that the antibodies used are specific for the intended KGDHC subunit proteins. It must be noted that in some panels, immunoreactivity with siRNA may appear similar

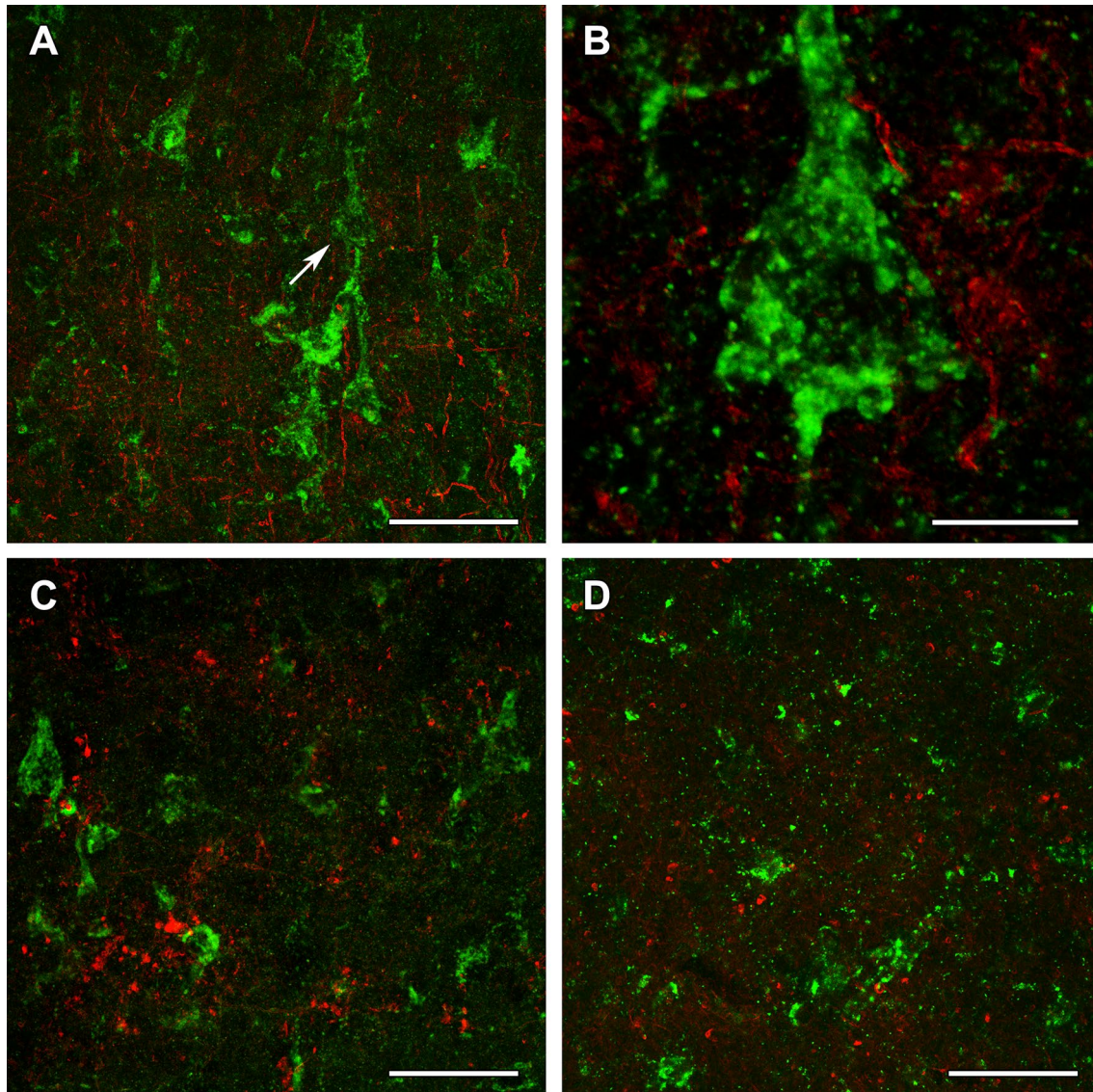


**Fig. 12** OGDHL and OGDH immunolabeling in the human cerebral cortex in relation to glial markers. **a** OGDHL-immunoreactive (green) cells as well as ALDH1-positive (red) astrocytes are both present in the cerebral cortex without any visible co-localization. **b** A high magnification confocal image of the area pointed to by the white arrow in **a** demonstrates that OGDHL-ir cells are not labeled

with Aldh1 and in turn, Aldh1-ir astrocytes do not contain OGDHL immunoreactivity. **c** Aldh1 (red) is also absent in OGDHL-ir cells and their processes (green). **d** The image demonstrates the lack of co-localization between OGDHL immunoreactivity (green) and the oligodendrocyte marker Olig2 (red). Scale bars = 50  $\mu\text{m}$  for **a**, **c**, and **d**, and 10  $\mu\text{m}$  for **b**

to immunoreactivity without any intervention; however, by semi-quantitating emitted light intensity of the signal minus the background, immunoreactivity presented for si RNA is consistently lower than that for scramble RNA (not shown).

Subsequently, to afford further assurance that the antibodies used exhibit monospecificity for the intended proteins—which cannot be addressed by immunocytochemistry—and they yield reproducible results from a sufficiently high number of tissues, we performed western blotting

analysis on purified, recombinant proteins (Nemeria et al. 2014; Ambrus et al. 2016) and 63 human brain homogenates obtained from 11 cadaveric brain donors. All antibodies are directed against short stretches of amino acid sequences (which was important for selecting isoform-specific antibodies), and thus, they were expected to perform equally well in western blotting protocols where protein folding is lost due to the presence of strong detergents. Antibody-selling company policies prohibit the publication of the epitopes (to which the authors disagree). As shown

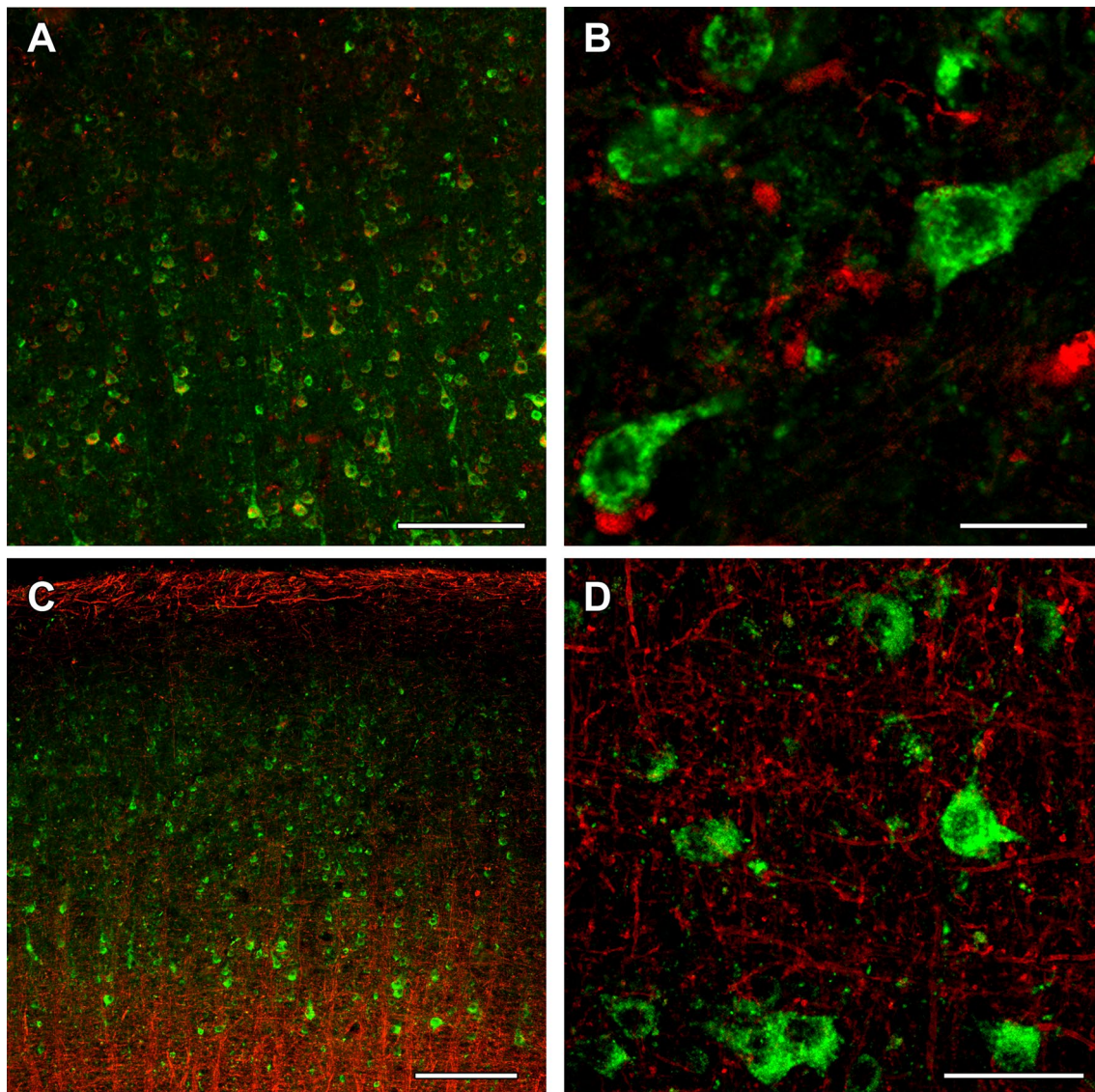


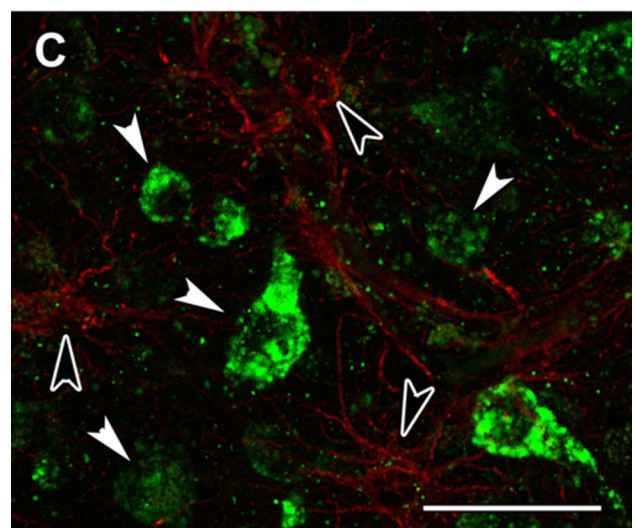
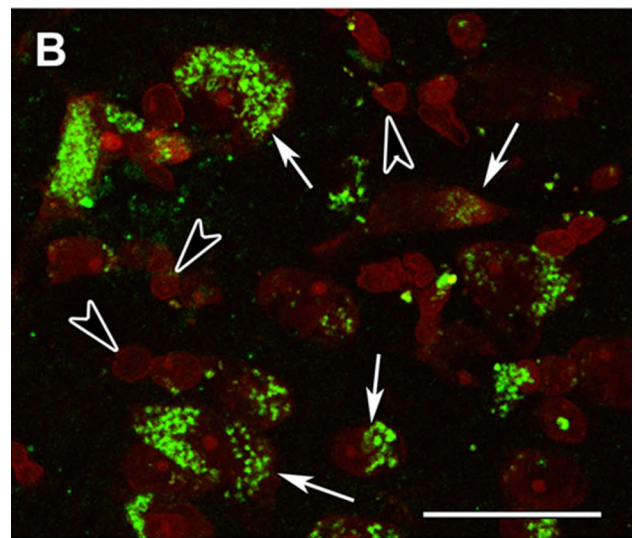
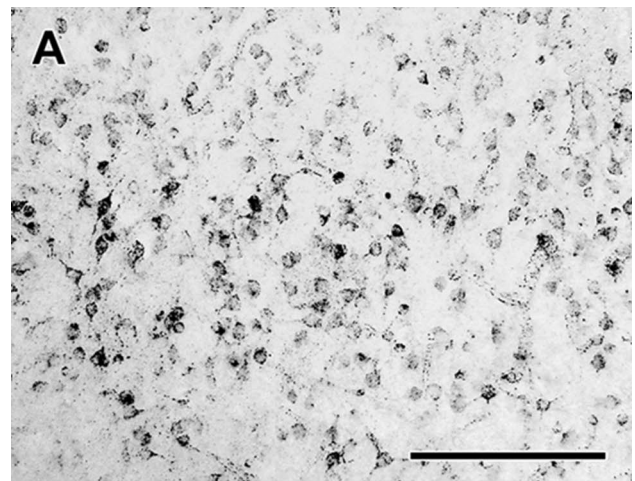
**Fig. 13** OGDH immunolabeling in the human cerebral cortex in relation to microglia and oligodendrocyte markers. **a** OGDH isoform 1/2 (green) and Iba1 (red) immunolabeling suggest a distinct distribution of OGDH-containing cells and microglia. In low magnification, OGDH- and IBA1-co-immunoreactivity may appear, but this notion is rejected in high magnification microphotographs. **b** A high magnification, optically 1  $\mu\text{m}$ -thick confocal image of a cerebral cortical section double stained with OGDH isoform 1/2 (green) and Iba1 (red) demonstrates that larger, neuronal cells are single labeled for OGDH

isoform 1/2. Several small cells are IBA1-positive. These cells are not labeled with OGDH isoform 1/2, suggesting that that microglial cells are negative for OGDH isoform 1/2. **c** A cerebral cortical section double labeled with OGDH isoform 1/2 (green) and the established oligodendrocyte marker myelin basic protein (MBP; red). The latter shows the typical distribution of myelinated fibers in the cerebral cortex. **d** A high magnification confocal image shows the lack of colocalization between OGDH isoform 1/2 and MBP-positive structures (red). Scale bars = 200  $\mu\text{m}$  for **a** and **c**, 25  $\mu\text{m}$  for **b**, and 50  $\mu\text{m}$  for **d**

in Fig. 9, recombinant proteins (shown on the left-most lane) and the brain homogenates were probed for SUCLG1, SUCLG2, SUCLA2, OGDH, DLST, DLD,  $\beta$ -actin, and VDAC1. Antibodies directed against OGDHL isoforms were not suitable for western blotting. Since the number of the homogenates used was higher than the number of lanes per gel that could be loaded, samples loaded in the last four lanes of each gel was also loaded in the first four lanes of the next gel.  $\beta$ -actin and VDAC1 served as loading

markers for total tissue homogenate and mitochondrial content, respectively. SUCLG1, SUCLG2, and SUCLA2 correspond to subunits of succinate-CoA ligase, the enzyme following KGDHC in the citric acid cycle. On the top lane, each three-digit number represents a brain homogenate sample from a brain donor. The exact brain location from where these homogenates originated is shown in Table 3. As shown in the cropped scanned western blots, the antibodies raised against OGDH, DLST, and DLD yielded a

**Fig. 14** DLST immunolabeling in the human cerebral cortex in relation to neuronal and glial markers. **a** DLST-immunoreactive (DLST-ir) cells are present in the cerebral cortex, with higher density in the deep layers. **b** DLST (green) and fluorescent Nissl staining (red) show that many cells are double-labeled in the cerebral cortex. Arrows point to double-labeled neurons, while black arrowheads point to single-labeled, DLST-immunonegative cells. Please note the dot-like distribution of DLST immunolabeling in the double-labeled neurons. **c** A cerebral cortical section double labeled with DLST (green) and the established astrocyte marker glial fibrillary acidic protein (GFAP; red) to show the lack of double labeling, suggesting that astrocytes are devoid of DLST. White arrowheads point to single-labeled (DLST-ir) neurons, while black arrowheads point to single-labeled (GFAP-ir) astrocytes. Scale bars = 300  $\mu\text{m}$  for **a**, and 30  $\mu\text{m}$  for **b** and **c**



band which appeared at the same molecular weight as the recombinant protein. Antibodies for SUCLG1, SUCLG2, and SUCLA2 have been validated elsewhere (Dobolyi et al. 2015a; b; Chinopoulos et al. 2018). Scanned images of whole blots appear in the supplemental material. In supplemental Fig. 1, it is shown that antibodies yielded—in the vast majority of cases—a single band at the expected molecular weight; when the blots were “overexposed”, several new bands appeared that were much fainter than the band corresponding to the intended protein. From the results shown in western blots and confocal imaging of immunocytochemistry, we concluded that the antibodies raised against KGDHC components are specific to the intended proteins. However, it must be emphasized that this did not apply for those raised against OGDHL isoforms.

#### **KGDHC subunit- and isoform-specific immunoreactivity in human brain cortex and cell types identification by co-staining with neuronal and/or glial markers**

Using the above validated antibodies, we performed immunohistochemistry in human cerebral cortical material obtained from neurosurgical interventions. Frontal and temporal cortical samples did not show any visible difference in their labeling pattern for any antibody. The distribution of OGDH subunits investigated with antibodies specific to different OGDHL and OGDH isoforms was similar (Figs. 10 and 11, respectively). Labeled cells were scarce in layer I of the cerebral cortex (Fig. 10a). In contrast, a high number of labeled cells were present in all other layers of the cerebral cortex (Fig. 10a and 11a). The labeling was absent in the nuclei of the cells, while it was punctate with occasional filamentous appearance in the perikarya. Although *in situ mitochondria* are filamentous, a largely punctate appearance emerged likely because of the multiple amplification steps. Furthermore, immunohistochemistry protocols of signal amplification almost always lead to diminished spatial resolution.

Thus, KGDHC staining in the human cerebral cortical tissue did not completely match the filamentous mitochondrial network commonly observed in cultured fibroblasts

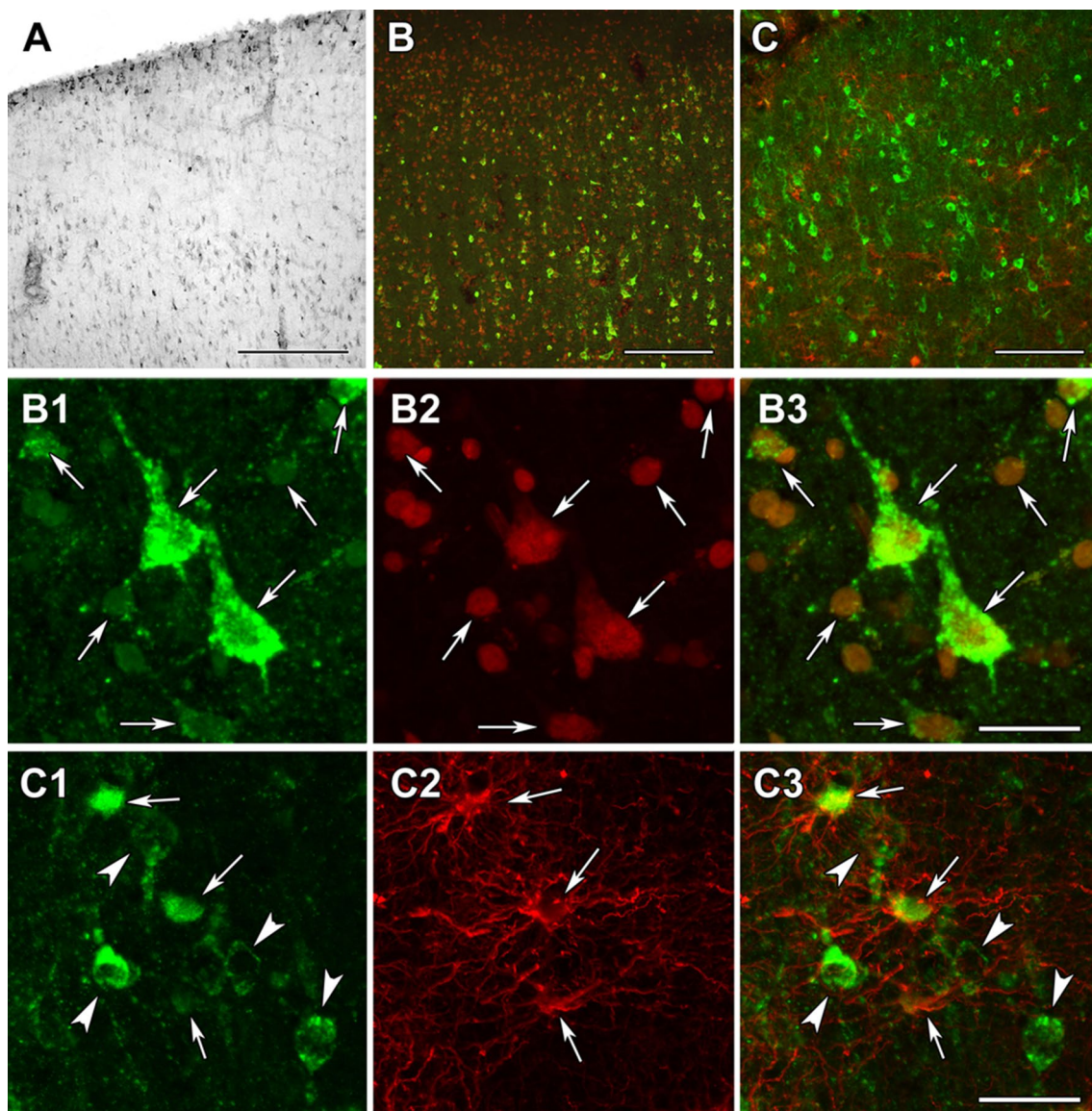


**Fig. 15** DLD immunolabeling in the human cerebral cortex in relation to neuronal and glial markers. **a** DLD-immunoreactive (DLD-ir) cells are present in layer 1 and also in deep layers of the cerebral cortex. The density of labeled cells is particularly high in layer 1 and the pyramidal layers. **b** DLD (green) and fluorescent Nissl staining (red) show that most cells are yellow, that is double-labeled in the cerebral cortex. **c** A cerebral cortical section double labeled with DLD (green) and the established astrocyte marker glial fibrillary acidic protein (GFAP; red) to show that most astrocyte contain DLD. **b1–3** A high magnification confocal image of the cerebral cortical section double

labeled with DLD (green) and fluorescent Nissl staining (red) demonstrates double labeling of the cells. The arrows point to some of the double-labeled cells. **b1** shows the green channel, **b2** the red channel, and **b3** the merged figure. **c1–3** A high magnification confocal image of the cerebral cortical section double labeled with DLD (green) and GFAP (red) demonstrates the presence of DLD in astrocytes (arrows). The arrowheads in turn point to neurons, which contain DLD, but do not express GFAP. **c1** shows the green channel, **c2** the red channel, and **c3** the merged figure. Scale bars = 300  $\mu\text{m}$  for **a**, 200  $\mu\text{m}$  for **b**, 100  $\mu\text{m}$  for **c**, and 20  $\mu\text{m}$  for **b1–3** and **c1–3**

and cell lines, but its appearance was still indicative of mitochondrial localization.

To identify the type of cells labeled with the different OGDH subtypes, double labeling was performed. A fluorescent Nissl dye allowed the analysis of cellular

morphology, which suggested the presence of all OGDH subtypes in neurons. In addition, a high number of smaller cells, also labeled with fluorescent Nissl dye, were also present, but did not contain OGDH. Since the smaller size and the even distribution of these cells suggested that

**Table 4** Immunoreactivity of OGDH (using antibody HPA019514) in the human brain according to Human Protein Atlas

KGDH complex subunit		OGDH											
Antibody		Atlas Antibodies Cat#HPA019514, RRID:AB_1854772											
Isoform specificity		Q02218-1, Q02218-2, Q02218-3											
Brain region	Gender (M/F)	Cerebral Cortex			Hippocampus			Caudate			Cerebellum		
		F	M	M	F	M	M	F	M	M	F	M	M
Age (years)		19	30	45	54	45	45	19	45	45	19	45	45
Glia (staining)		Low	Low	Low	Low	Low	Low	Low	Low	Low	Low	Low	Low (molecular layer)
Neurons (staining)		High	High	High	Medium	Medium	Medium	Medium	Medium	Medium	Medium	Medium	Low granular layer, High Purkinje cells

**Table 5** Immunoreactivity of OGDH (using antibody HPA020347) in the human brain according to Human Protein Atlas

KGDH complex subunit		OGDH											
Antibody		Atlas Antibodies Cat#HPA020347, RRID:AB_1854773											
Isoform specificity		Q02218-1, Q02218-2, Q02218-3											
Brain region	Gender (M/F)	Cerebral Cortex			Hippocampus			Caudate			Cerebellum		
		F	M	M	F	M	M	F	M	M	F	M	M
Age (years)		19	30	57	54	45	45	45	45	45	70	19	54
Glia (staining)		Low	Low	Low	Medium	Medium	High	High	High	High	High	Medium (molecular layer)	Medium (molecular layer)
Neurons (staining)		High	High	High	Medium	Medium	Medium	Medium	Medium	Medium	High (granular layer and Purkinje cells)	High (granular layer and Purkinje cells)	High (granular layer and Purkinje cells)

**Table 6** Immunoreactivity of OGDHL in the human brain according to Human Protein Atlas

KGDH complex subunit		OGDHL											
Antibody		Atlas Antibodies Cat#HPA052497, RRID:AB_2681853											
Isoform specificity		Q9ULD0-1											
Brain region		Cerebral cortex				Caudate				Cerebellum			
Gender (M/F)		M	M	M	M	F	F	F	F	M	M	M	M
Age (years)	6	37	70	42	52	64	37	58	70	19	54	54	54
Glia (staining)	Low	Low	Low	N.D.	N.D.	N.D.	N.D.	N.D.	N.D.	High (molecular layer)	High (molecular layer)	High (molecular layer)	High (molecular layer)
Neurons (staining)	Medium	Medium	Medium	Low	Low	Low	Medium	Medium	Medium	High (Purkinje cells and granular layer)			

*N.D.*, not detected

**Table 7** Immunoreactivity of DLST in the human brain according to Human Protein Atlas

KGDH complex subunit		DLST															
Antibody		Atlas Antibodies Cat#HPA003010, RRID:AB_1078679															
Isoform specificity		P36957-1, P36957-2															
Brain region		Cerebral Cortex				Hippocampus				Caudate				Cerebellum			
Gender (M/F)		F	F	M	M	F	F	M	M	F	F	M	M	F	F	M	M
Age (years)	45	54	45	45	19	54	45	19	54	45	19	45	45	19	45	45	45
Glia (staining)	Low	Low	Low	Low	Medium	Medium	Medium	Medium	Medium	Medium	Medium	Medium	Medium	Medium	Medium	Medium	Medium (molecular layer)
Neurons (staining)	Medium	Medium	Medium	Medium	Medium	Medium	Medium	Medium	Medium	Medium	Medium	N. INF.	N. INF.	N. INF.	Low in granular layer, high in Purkinje cells	Low in granular layer, high in Purkinje cells	Low in granular layer, high in Purkinje cells

*N.INF.*, no information



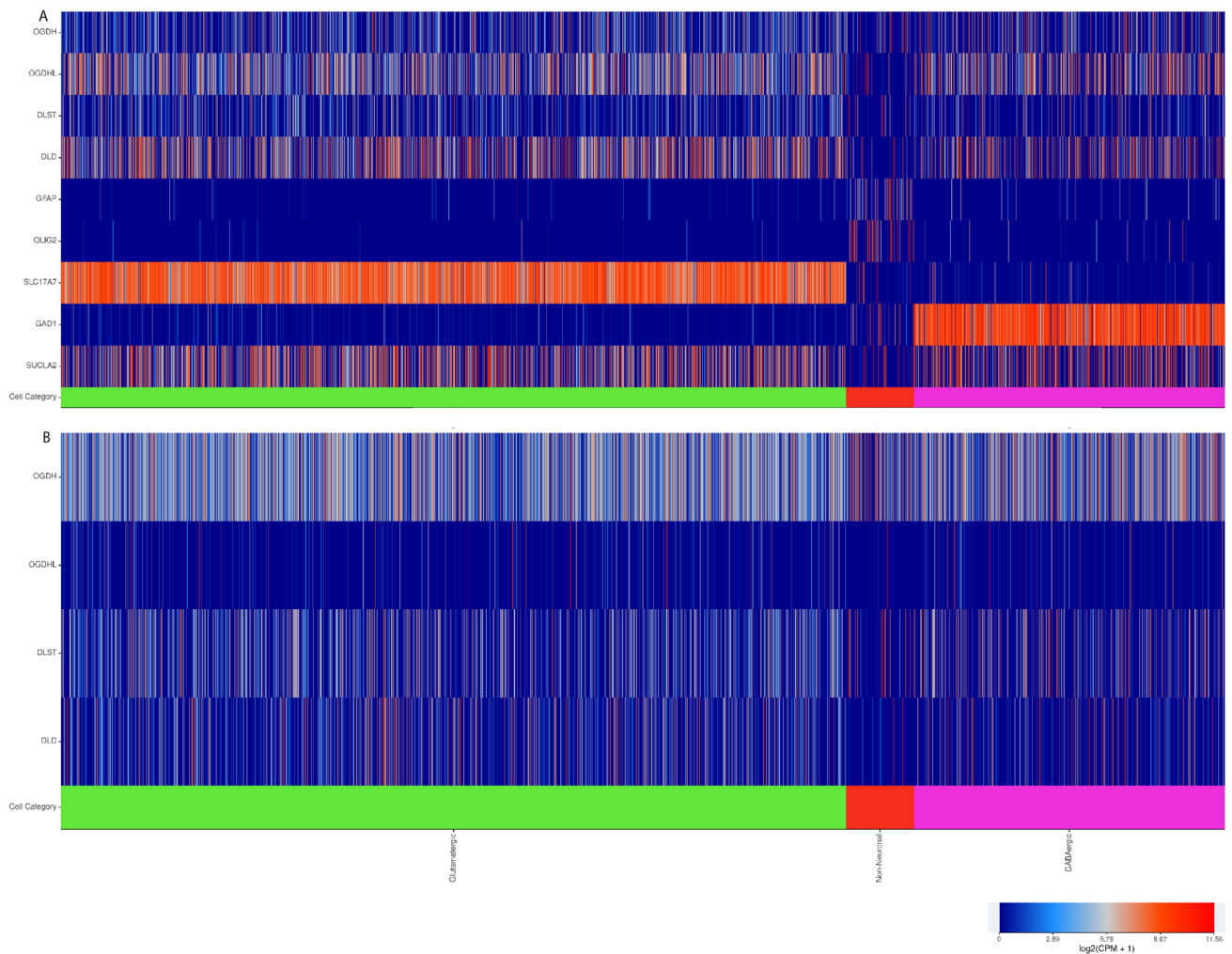


**Fig. 16** RNA-Seq data obtained from the Allen Brain Atlas, looking at the expression of genes indicated in the left, as a function of cell types. **a** Genes found only in exons. **b** Genes found only in introns. Image credit: Allen Institute. <https://celltypes.brain-map.org/rnaseq/human>

Protein Atlas, namely that KGDHC-specific subunits are expressed in neurons and little (if at all) in cortical glia.

### Correlation of immunohistochemistry results obtained in this study from KGDHC subunit staining and RNA-Seq data published in the Allen Brain Atlas

The Allen Brain Atlas is an integrated spatio-temporal portal for exploring the central nervous system (Sunkin et al. 2013). It entails—among other databases—RNA-Seq data from intact nuclei derived from frozen human brain specimens obtained from middle temporal gyri. Specifically, 15,928 nuclei from 8 human tissue donors ranging in age from 24–66 years were analyzed. As shown in Fig. 16a, RNA-Seq data for OGDH, OGDHL, DLST, and DLD (indicated on the left) are shown as a function of cell subtype (indicated in the *x*-axis). These data are pooled exclusively from the

exons. It is immediately apparent that, in non-neuronal cells, thus including glia- expression of KGDHC components is much less than that in glutamatergic + GABA-ergic cells, i.e., collectively neuronal cells. For comparisons, RNA-Seq data for GFAP and Olig2 (glial markers), SLC17A7 (Solute Carrier Family 1 (Glutamate Transporter), Member 7; it transports L-glutamate; glutamatergic neuron marker), GAD1: Glutamate Decarboxylase isoform 1; GABA-ergic neuronal marker and SUCLA2 (component of ATP-forming succinate-CoA ligase, neuronal marker) are also presented. On the other hand, in Fig. 16b, RNA-Seq data from introns only are presented, and there, it is apparent that gene elements coding for KGDHC components are essentially the same between neuronal vs non-neuronal cells; this practically means that in non-neuronal cells (such as glia), genes coding for KGDHC components are embedded in intronic regions as a result of some genetic regulation.

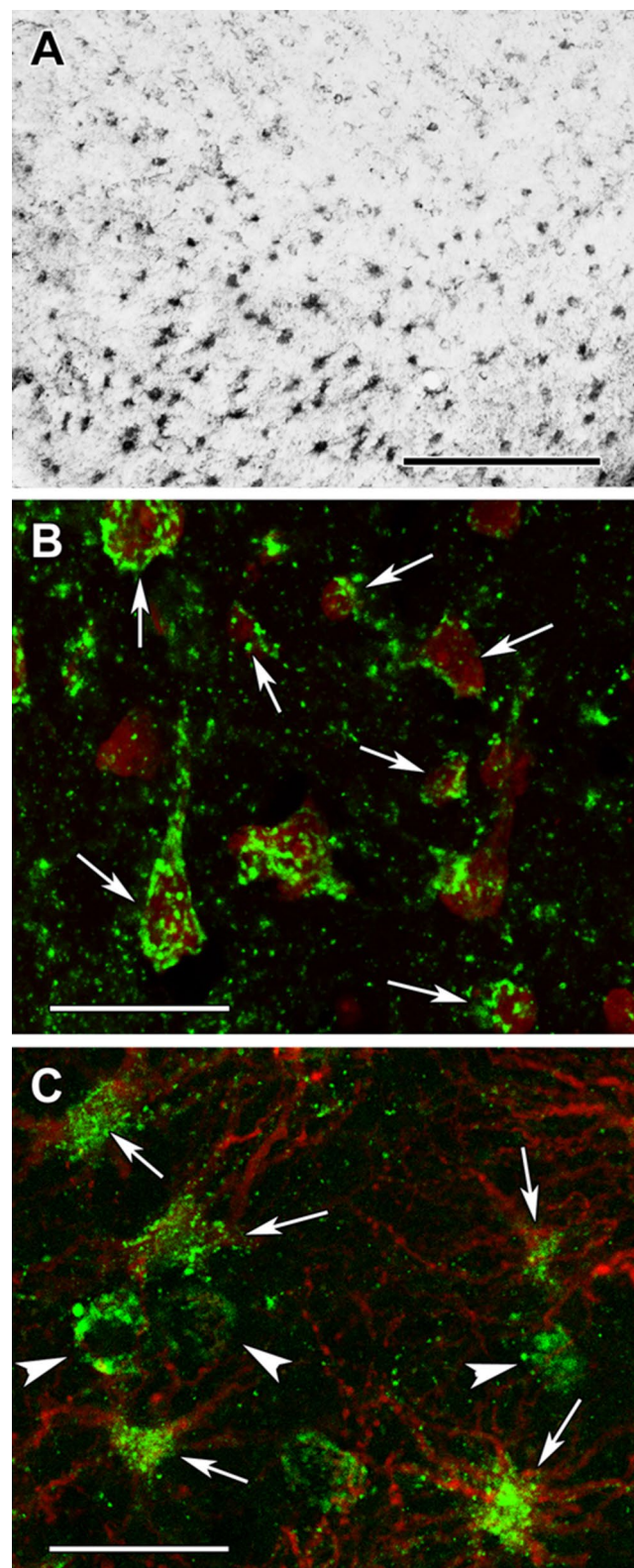
**Fig. 17** Succinyl-lysine immunolabeling in the human cerebral cortex in relation to neuronal and glial markers. **a** Succinyl-lysine-immunoreactive (SUCCLYS-ir) cells are present in the cerebral cortex, with higher density in the deep layers. **b** Succinyl-lysine (green) and fluorescent Nissl staining (red) show that essentially all cells are double-labeled in the cerebral cortex. Arrows point to some of these double-labeled cells. Note the dot-like distribution of succinyl-lysine immunolabeling in the double-labeled cells. **c** A cerebral cortical section double labeled with succinyl-lysine (green) and the established astrocyte marker glial fibrillary acidic protein (GFAP; red) to show the double labeling of astrocytes. White arrowheads point to single-labeled (SUCCLYS-ir) neurons. Scale bars = 300  $\mu$ m for **a** and 30  $\mu$ m for **b** and **c**

### Protein lysine succinylation is pancellularly evident in the human brain

All cells in the examined cerebral cortices were immunopositive for protein lysine succinylation (Fig. 17a) as demonstrated by the lack of cells singly labelled with the fluorescent Nissl dye (Fig. 17b). The localization in astrocytes was also confirmed by double labeling with GFAP as indeed all GFAP-positive glial cells contained immunolabeling for protein lysine succinylation, as well (Fig. 17c). The specificity of the labeling was confirmed by the absence of signal when the antibody was pre-incubated with succinylated Wheat Germ Agglutinin (WGA, Fig. 18b, d) but not WGA without succinylation Fig. 18a, c). Specificity of the anti-succinyllysine antibody was further assured by an independent methodology, Western blotting (WB) of homogenized brains. As shown in Fig. 18e–h, WB for 12 different brain homogenates was performed. In the same gels, wheat germ agglutinin (WGA) and succinylated WGA were loaded where indicated. In panel E, blots were probed with anti-succinyllysine antibody; the blot shown in panel F was treated with anti-succinyllysine antibody plus WGA; the blot shown in panel G was treated with anti-succinyllysine antibody plus succinylated WGA; and the blot strip shown in panel H depicts the result of probing for  $\beta$ -actin, as loading control. It is evident that incubation of the anti-succinyllysine antibody with succinylated WGA (Fig. 18g) but not WGA (Fig. 18f) yields very little staining. WGA contains endogenous succinylated sites (Zhang et al. 2017), and thus, a band is visible in the respective lane.

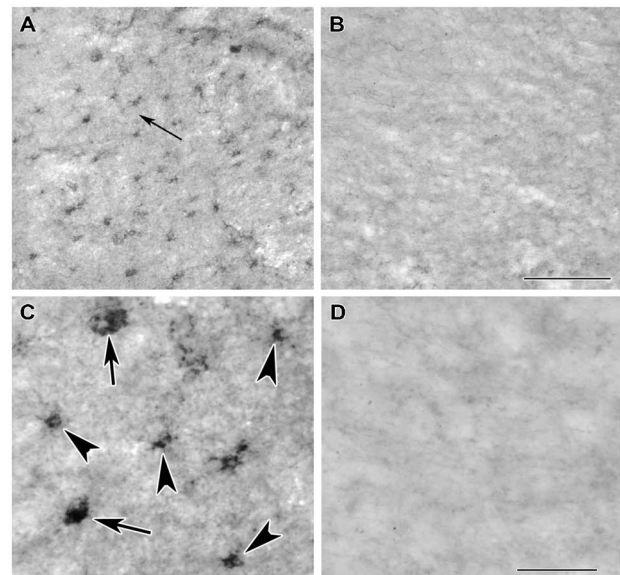
### Proposed metabolic differences (pertinent to KGDHC) between neurons and glia in the adult human cortex

The above results indicate that glia of the human brain lack KGDHC. Mindful of the previously published work shows that they also lack succinate-CoA ligase (Dobolyi et al. 2015a; b), and the segment of the citric acid cycle from  $\alpha$ -ketoglutarate to succinate could only be connected through the GABA shunt, a pathway which is known to



take place in glia (Minelli et al. 1996; Conti et al. 1998, 1999). However, succinyl-CoA is still being made since protein lysine succinylations were detected in these cells as well. Thus, we propose the following metabolism

**Fig. 18** Testing of the specificity of the anti-succinyl-lysine antibody by absorption in the human cerebral cortex. **a** Preincubation of the anti-succinyl-lysine antibody with wheat germ agglutinin does not prevent immunolabeling. The arrow indicates the area magnified in **c**. **b** Following preincubation of the anti-succinyl-lysine antibody with succinylated wheat germ agglutinin, no labeled cells are present suggesting that the preincubation eliminates specific immunolabeling in a section adjacent to the one shown in **a**. **c, d** Higher magnification images confirm the effect of preabsorption with succinylated wheat germ agglutinin. Note the different types of labelled cells in **c** as arrows point to larger cells, probably neurons while arrowheads point to small cells with several processes resembling glial cells. Scale bars = 200  $\mu\text{m}$  for **a** and **b**, and 50  $\mu\text{m}$  for **c** and **d**. **e** Western blot loaded with 12 brain homogenates, WGA-loaded lane and succinylated WGA, where indicated, treated with anti-succinyllysine. **f** Same as for **e**, treated with WGA plus anti-succinyllysine. **g** Same as for **e** but treated with succinylated WGA plus anti-succinyllysine, which effectively eliminated the labeling. **h**  $\beta$ -actin as loading control

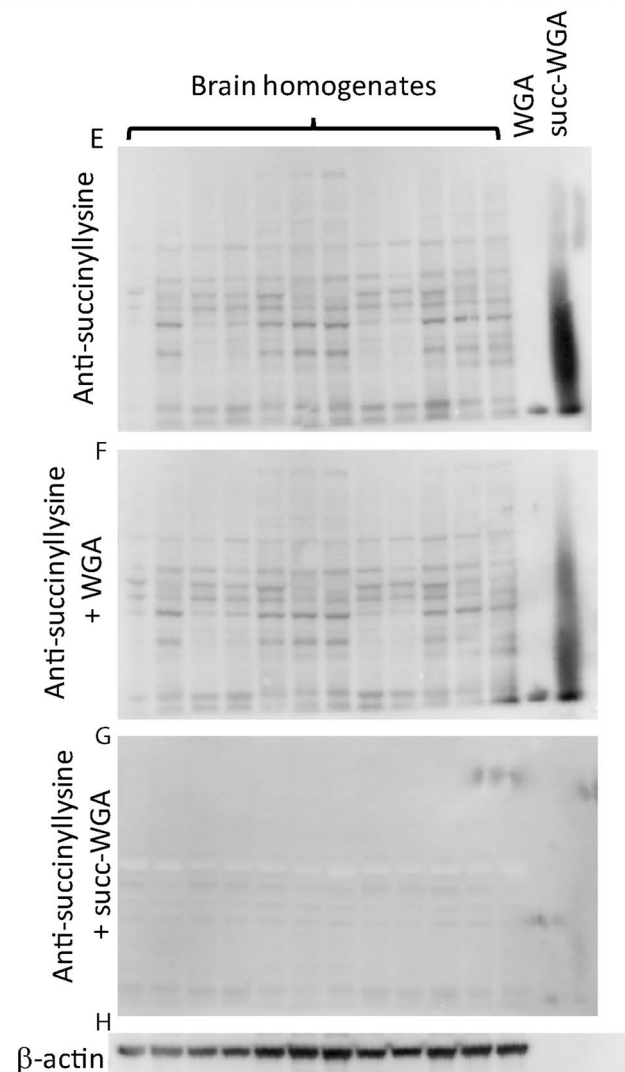


pertinent to KGDHC in neurons versus glia: as shown in Fig. 19, neuronal mitochondria (blue box) perform the citric acid cycle as described in textbooks. They also receive glutamine (Gln) from the extracellular space (EC), which originated from glia as part of the so-called “glutamate–glutamine cycle” between neurons and glia (Sonnewald and Schousboe 2016). Some neurons will also extrude GABA to the EC, which can be taken up by the glia. Glial mitochondria (orange box), on the other hand, will also take up glutamate from the EC, which has been released by neurons and further process it by transamination or use it for forming GABA. Succinyl-CoA in glia can only be produced from valine, isoleucine, methionine, thymine, odd-number chain fatty acids, and, perhaps, propionate (multiple reactions, omitted for clarity), and from the reaction catalyzed by OXCT1, an enzyme participating in ketone bodies catabolism; relevant to this, ketone bodies metabolism is known to occur in human astrocytes (Thevenet et al. 2016).

## Discussion

The two most important observations of the present work are that (1) we detected KGDHC-specific subunits immunoreactivity in neurons but not glia of the human brain, and (2) protein lysine succinylations were pancellularly observed, thus, in glia, succinyl-CoA is probably a product of an enzyme other than KGDHC. Furthermore, to the best of our knowledge, our work is the first to demonstrate protein lysine succinylation in the adult human cortex. DLD subunit was found also in non-neuronal cells, but this is probably due to its participation in the pyruvate dehydrogenase complex, branched-chain alpha-keto acid dehydrogenase complex, and the glycine cleavage system.

Regarding the finding that KGDHC-specific components were not observed in cells staining positive with



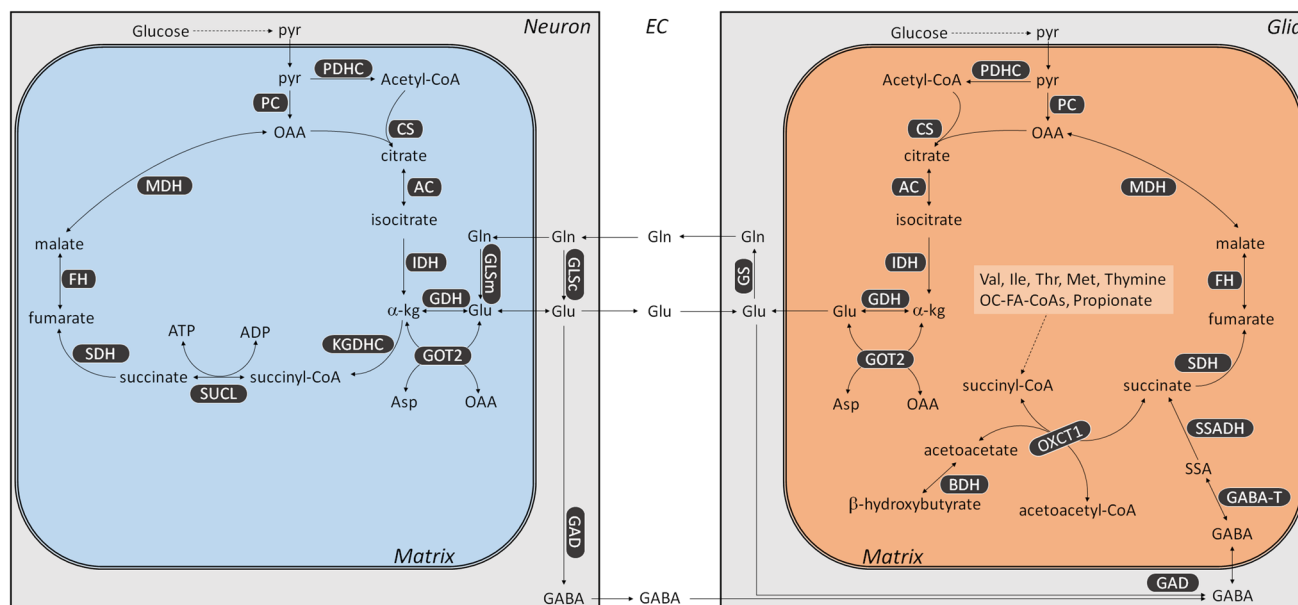


**Fig. 19** Metabolic considerations of a neuronal mitochondrion (blue box) and a glial mitochondrion (orange box) pertinent to KGDHC. *AC* aconitase, *BDH*  $\beta$ -hydroxybutyrate dehydrogenase, *CS* citrate synthase, *FH* fumarase, *GAD* glutamate decarboxylase, *GABA-T* GABA aminotransferase, *GDH* glutamate dehydrogenase, *GLSc* glutaminase (cytosolic), *GLSm* glutaminase (mitochondrial), *GOT2* aspartate ami-

notransferase, *IDH* isocitrate dehydrogenase, *KGDHC* ketoglutarate dehydrogenase complex, *MDH* malate dehydrogenase (mitochondrial), *OXCT1* succinyl-CoA:3-oxoacid CoA-transferase, *PC* pyruvate carboxylase, *PDHC* pyruvate dehydrogenase complex, *SDH* succinate dehydrogenase, *SSADH* succinic semialdehyde dehydrogenase, *SUCL* succinyl-CoA ligase

glial markers, it is important to emphasize that our immunohistochemistry protocols included several amplification steps. This implies that if KGDHC-specific components are expressed in human glia, they are probably at least two orders of magnitude less abundant than those expressed in neurons, precluding the possibility of an appreciable KGDHC activity in the former cell types. The group of John P Blass has also published the absence of KGDHC immunoreactivity from glia in the adult human brain; however, out of perhaps abundance of caution, they reported it as “surprisingly, convincing immunoreactivity was not found in glia” (Ko et al. 2001), even though KGDHC immunoreactivity was completely absent from all of their microphotographs. Here, we investigated glial cells exhibiting GFAP, Aldh1l, myelin basic protein, Olig2, and IBA1, identifying astrocytes, oligodendrocytes, and microglia. However, the human brain harbors hundreds (if not thousands) of cell types and subtypes. The Human Brain Project aims to identify and catalogue all these cells (Amunts et al. 2016). Thus, it cannot be excluded that some glial subtypes exhibit KGDHC-specific components to a detectable level. This is supported by RNA-Seq data obtained from the Allen Brain Atlas, in which positive “hits” were scarce but still visible in non-neuronal cells. The notion that glia of the adult human brain may not exhibit KGDHC (nor succinyl-CoA ligase) activity, thus precluding operation of the citric acid cycle as we know it calling for reconsideration of a textbook definition of a universal

metabolic pathway should not come as a great surprise: mice engineered to lack cytochrome c oxidase in astrocytic mitochondria in vivo were fully viable in the absence of any signs of glial or neuronal loss even at 1 year of age (Supplie et al. 2017). Notably though, KGDHC (detected immunologically using an antibody generated using the whole complex as an epitope) has been reported in astrocytes of cerebrum and cerebellum of newborn mice (Waagepetersen et al. 2006). Furthermore, in (Calingasan et al. 1994), it was shown that in 3-month-old male Fischer 344/Brown Norway F1 hybrid rats immunohistochemistry for KGDHC (using an anti-rabbit IgG for KGDHC, no further information is provided), KGDHC stained neurons much more intensely than glia in several brain areas. Perhaps, KGDHC is absent (or at least present at an extremely small level) in human glia so as to assist the glutamate-glutamine cycle by preventing glutamate catabolism through the citric acid cycle (which necessitates KGDHC activity), instead being shuttled towards glutamine formation. By the same token, glutamate taken up from the EC would be shuttled towards GABA metabolism, also known to operate in glia cells. Relevant to this, in a human embryonic kidney cell line, even a mild reduction (~30%) in KGDHC activity elevated the GABA shunt (Shi et al. 2009).

Regarding the observation of pancellular lysine succinylation in the adult human cortex in view of the fact that glia may not exhibit KGDHC nor succinyl-CoA ligase

activity implies that these cells must obtain succinyl-CoA from some other metabolic pathway. Succinylations are widespread and may occur in an enzymatic (Gibson et al. 2015; Wang et al. 2017; Kurmi et al. 2018) and non-enzymatic (Wagner and Payne 2013; Weinert et al. 2013) manner. However, they all require succinyl-CoA. In mammals, this high-energy metabolite can be generated only through KGDHC, succinyl-CoA ligase, catabolism of valine, isoleucine, methionine, thymine, odd-number chain fatty acids (and perhaps propionate), and through the reaction catalyzed by OXCT1. Since glia may not exhibit KGDHC nor succinyl-CoA ligase components, provision of succinyl-CoA is ensured only by the remaining pathways. Mindful of the remaining pathways generating succinyl-CoA inside the matrix, it is still a mystery how can there be extramitochondrial protein lysine succinylations. KGDHC components have been observed in the nuclei of the human cell line U251 (Wang et al. 2017), in rat neonatal cardiac myocytes, human-induced pluripotent stem cardiac myocytes, SW620 human colon cancer cells, and developing mouse embryonic heart (Choi et al. 2019); however, we did not observe KGDHC subunit immunoreactivity in the nuclei of our human fibroblasts, HeLa, and COS-7 cells, nor in the human cortical sections.

**Acknowledgements** Open access funding provided by Semmelweis University (SE). We appreciate the technical contribution of Erzsébet Horváthné Oszwald.

**Author contributions** CC Designed research; AD, AB, JD, and CC performed research, MP, NSN, FJ, AA, and VA-V contributed materials/reagents; AD and CC analyzed data; AD and CC wrote the paper.

**Funding** This work was supported by the NIH [GM050380] and [R15-GM116077] to F.J., Hungarian Academy of Sciences [02001], Hungarian Scientific Research Fund [OTKA 112230], Hungarian Brain Research Program [KTIA\_13\_NAP-A-III/6. and 2017-1.2.1-NKP-2017-00002], and Hungarian Higher Education Institution Excellence Program [FIKP 61822 64860 EATV] to V. A.-V. and FIKP [61826 690289 EATV] to A.A., NKFIH-4300-1/2017-NKP\_17 to A.D. and Grants FIKP-61822-64888-EATV, VEKOP 2.3.3-15-2016-00012, 2017-2.3.4-TET-RU-2017-00003, and NKFIH KH129567 to C.C.

## Compliance with ethical standards

**Conflict of interest** The authors declare no competing financial interests.

**Research involving human participants and/or animals** All procedures performed in studies involving human participants were in accordance with the ethical standards of the institutional and/or national research committee and with the 1964 Helsinki declaration and its later amendments or comparable ethical standards (see under “Materials and Methods”, *Human Brains*). This article does not contain any studies with animals performed by any of the authors.

**Informed consent** Informed consent was obtained from all individual participants included in the study, and/or (in case of *post-mortem* brain

donors) from the next of kin (see under “Materials and Methods”, *Human Brains*).

**Open Access** This article is licensed under a Creative Commons Attribution 4.0 International License, which permits use, sharing, adaptation, distribution and reproduction in any medium or format, as long as you give appropriate credit to the original author(s) and the source, provide a link to the Creative Commons licence, and indicate if changes were made. The images or other third party material in this article are included in the article’s Creative Commons licence, unless indicated otherwise in a credit line to the material. If material is not included in the article’s Creative Commons licence and your intended use is not permitted by statutory regulation or exceeds the permitted use, you will need to obtain permission directly from the copyright holder. To view a copy of this licence, visit <http://creativecommons.org/licenses/by/4.0/>.

## References

- Albers DS, Augood SJ, Park LC, Browne SE, Martin DM, Adamson J, Hutton M, Standaert DG, Vonsattel JP, Gibson GE, Beal MF (2000) Frontal lobe dysfunction in progressive supranuclear palsy: evidence for oxidative stress and mitochondrial impairment. *J Neurochem* 74(2):878–881
- Ambrus A, Wang J, Mizsei R, Zambo Z, Torocsik B, Jordan F, Adam-Vizi V (2016) Structural alterations induced by ten disease-causing mutations of human dihydrolipoamide dehydrogenase analyzed by hydrogen/deuterium-exchange mass spectrometry: implications for the structural basis of E3 deficiency. *Biochim Biophys Acta* 1862(11):2098–2109. <https://doi.org/10.1016/j.bbadis.2016.08.013>
- Amunts K, Ebell C, Muller J, Telefont M, Knoll A, Lippert T (2016) The human brain project: creating a European research infrastructure to decode the human brain. *Neuron* 92(3):574–581. <https://doi.org/10.1016/j.neuron.2016.10.046>
- Atamna H, Frey WH (2004) A role for heme in Alzheimer’s disease: heme binds amyloid beta and has altered metabolism. *Proc Natl Acad Sci USA* 101(30):11153–11158
- Atamna H, Liu J, Ames BN (2001) Heme deficiency selectively interrupts assembly of mitochondrial complex IV in human fibroblasts: relevance to aging. *J Biol Chem* 276(51):48410–48416
- Bubber P, Haroutunian V, Fisch G, Blass JP, Gibson GE (2005) Mitochondrial abnormalities in Alzheimer brain: mechanistic implications. *Ann Neurol* 57(5):695–703
- Bubber P, Hartounian V, Gibson GE, Blass JP (2011) Abnormalities in the tricarboxylic acid (TCA) cycle in the brains of schizophrenia patients. *Eur Neuropsychopharmacol* 21(3):254–260
- Burch JS, Marcero JR, Maschek JA, Cox JE, Jackson LK, Medlock AE, Phillips JD, Dailey HA Jr (2018) Glutamine via alpha-ketoglutarate dehydrogenase provides succinyl-CoA for heme synthesis during erythropoiesis. *Blood* 132(10):987–998. <https://doi.org/10.1182/blood-2018-01-829036>
- Butterworth RF, Besnard AM (1990) Thiamine-dependent enzyme changes in temporal cortex of patients with Alzheimer’s disease. *Metab Brain Dis* 5(4):179–184
- Butterworth RF, Kril JJ, Harper CG (1993) Thiamine-dependent enzyme changes in the brains of alcoholics: relationship to the Wernicke-Korsakoff syndrome. *Alcohol Clin Exp Res* 17(5):1084–1088
- Calingasan NY, Baker H, Sheu KF, Gibson GE (1994) Distribution of the alpha-ketoglutarate dehydrogenase complex in rat brain. *J Comp Neurol* 346(3):461–479

- Chen Z, Zhong C (2013) Decoding Alzheimer's disease from perturbed cerebral glucose metabolism: implications for diagnostic and therapeutic strategies. *Prog Neurobiol* 108:21–43. <https://doi.org/10.1016/j.pneurobio.2013.06.004>
- Chinopoulos C (2013) Which way does the citric acid cycle turn during hypoxia? The critical role of alpha-ketoglutarate dehydrogenase complex. *J Neurosci Res* 91(8):1030–1043
- Chinopoulos C, Batzios S, van den Heuvel LP, Rodenburg R, Smeets R, Waterham HR, Turkenburg M, Ruiten JP, Wanders RJA, Doczi J, Horvath G, Dobolyi A, Vargiami E, Wevers RA, Zafeiriou D (2018) Mutated SUCLG1 causes mislocalization of SUCLG2 protein, morphological alterations of mitochondria and an early-onset severe neurometabolic disorder. *Mol Genet Metab*. <https://doi.org/10.1016/j.ymgme.2018.11.009>
- Choi S, Pfeleger J, Jeon YH, Yang Z, He M, Shin H, Sayed D, Astrof S, Abdellatif M (2019) Oxoglutarate dehydrogenase and acetyl-CoA acyltransferase 2 selectively associate with H2A.Z-occupied promoters and are required for histone modifications. *Biochim Biophys Acta Gene Regul Mech* 1862(10):194436. <https://doi.org/10.1016/j.bbagr.2019.194436>
- Conti F, Melone M, De BS, Minelli A, Brecha NC, Ducati A (1998) Neuronal and glial localization of GAT-1, a high-affinity gamma-aminobutyric acid plasma membrane transporter, in human cerebral cortex: with a note on its distribution in monkey cortex. *J Comp Neurol* 396(1):51–63
- Conti F, Zuccarello LV, Barbaresi P, Minelli A, Brecha NC, Melone M (1999) Neuronal, glial, and epithelial localization of gamma-aminobutyric acid transporter 2, a high-affinity gamma-aminobutyric acid plasma membrane transporter, in the cerebral cortex and neighboring structures. *J Comp Neurol* 409(3):482–494
- Cooney GJ, Taetgmeier H, Newsholme EA (1981) Tricarboxylic acid cycle flux and enzyme activities in the isolated working rat heart. *Biochem J* 200(3):701–703. <https://doi.org/10.1042/bj2000701>
- Cooper AJ (2012) The role of glutamine synthetase and glutamate dehydrogenase in cerebral ammonia homeostasis. *Neurochem Res* 37(11):2439–2455
- Dobolyi A, Bago AG, Gal A, Molnar MJ, Palkovits M, Adam-Vizi V, Chinopoulos C (2015a) Localization of SUCLA2 and SUCLG2 subunits of succinyl CoA ligase within the cerebral cortex suggests the absence of matrix substrate-level phosphorylation in glial cells of the human brain. *J Bioenerg Biomembr* 47(1–2):33–41
- Dobolyi A, Ostergaard E, Bago AG, Doczi T, Palkovits M, Gal A, Molnar MJ, Adam-Vizi V, Chinopoulos C (2015b) Exclusive neuronal expression of SUCLA2 in the human brain. *Brain Struct Funct* 220(1):135–151. <https://doi.org/10.1007/s00429-013-0643-2>
- Dumont M, Ho DJ, Calingasan NY, Xu H, Gibson G, Beal MF (2009) Mitochondrial dihydrolipoyl succinyltransferase deficiency accelerates amyloid pathology and memory deficit in a transgenic mouse model of amyloid deposition. *Free Radic Biol Med* 47(7):1019–1027
- Gibson GE, Starkov A, Blass JP, Ratan RR, Beal MF (2010) Cause and consequence: mitochondrial dysfunction initiates and propagates neuronal dysfunction, neuronal death and behavioral abnormalities in age-associated neurodegenerative diseases. *Biochim Biophys Acta* 1802(1):122–134
- Gibson GE, Sheu KF, Blass JP, Baker A, Carlson KC, Harding B, Perrino P (1988) Reduced activities of thiamine-dependent enzymes in the brains and peripheral tissues of patients with Alzheimer's disease. *Arch Neurol* 45(8):836–840
- Gibson GE, Zhang H, Sheu KF, Bogdanovich N, Lindsay JG, Lannfelt L, Vestling M, Cowburn RF (1998) Alpha-ketoglutarate dehydrogenase in Alzheimer brains bearing the APP670/671 mutation. *Ann Neurol* 44(4):676–681
- Gibson GE, Park LC, Sheu KF, Blass JP, Calingasan NY (2000) The alpha-ketoglutarate dehydrogenase complex in neurodegeneration. *Neurochem Int* 36(2):97–112
- Gibson GE, Kingsbury AE, Xu H, Lindsay JG, Daniel S, Foster OJ, Lees AJ, Blass JP (2003) Deficits in a tricarboxylic acid cycle enzyme in brains from patients with Parkinson's disease. *Neurochem Int* 43(2):129–135
- Gibson GE, Hirsch JA, Cirio RT, Jordan BD, Fonzetti P, Elder J (2013) Abnormal thiamine-dependent processes in Alzheimer's disease lessons from diabetes. *Mol Cell Neurosci* 55:17–25. <https://doi.org/10.1016/j.mcn.2012.09.001>
- Gibson GE, Xu H, Chen HL, Chen W, Denton TT, Zhang S (2015) Alpha-ketoglutarate dehydrogenase complex-dependent succinylation of proteins in neurons and neuronal cell lines. *J Neurochem* 134(1):86–96. <https://doi.org/10.1111/jnc.13096>
- Johnson JD, Mehus JG, Tews K, Milavetz BI, Lambeth DO (1998) Genetic evidence for the expression of ATP- and GTP-specific succinyl-CoA synthetases in multicellular eucaryotes. *J Biol Chem* 273(42):27580–27586
- Kiss G, Konrad C, Doczi J, Starkov AA, Kawamata H, Manfredi G, Zhang SF, Gibson GE, Beal MF, Adam-Vizi V, Chinopoulos C (2013) The negative impact of alpha-ketoglutarate dehydrogenase complex deficiency on matrix substrate-level phosphorylation. *FASEB J* 27(6):2392–2406
- Ko LW, Sheu KF, Thaler HT, Markesbery WR, Blass JP (2001) Selective loss of KGDHC-enriched neurons in Alzheimer temporal cortex: does mitochondrial variation contribute to selective vulnerability? *J Mol Neurosci* 17(3):361–369
- Kurmi K, Hitosugi S, Wiese EK, Boakye-Agyeman F, Gonsalves WI, Lou Z, Karnitz LM, Goetz MP, Hitosugi T (2018) Carnitine palmitoyltransferase 1A Has a lysine succinyltransferase activity. *Cell Rep* 22(6):1365–1373. <https://doi.org/10.1016/j.celrep.2018.01.030>
- Maas E, Bisswanger H (1990) Localization of the alpha-oxoacid dehydrogenase multienzyme complexes within the mitochondrion. *FEBS Lett* 277(1–2):189–190
- Mastrogiacono F, Lindsay JG, Bettendorff L, Rice J, Kish SJ (1996) Brain protein and alpha-ketoglutarate dehydrogenase complex activity in Alzheimer's disease. *Ann Neurol* 39(5):592–598. <https://doi.org/10.1002/ana.410390508>
- Minelli A, DeBiasi S, Brecha NC, Zuccarello LV, Conti F (1996) GAT-3, a high-affinity GABA plasma membrane transporter, is localized to astrocytic processes, and it is not confined to the vicinity of GABAergic synapses in the cerebral cortex. *J Neurosci* 16(19):6255–6264
- Naseri NN, Xu H, Bonica J, Vonsattel JP, Cortes EP, Park LC, Arjomand J, Gibson GE (2015) Abnormalities in the tricarboxylic acid cycle in Huntington disease and in a Huntington disease mouse model. *J Neuropathol Exp Neurol* 74(6):527–537. <https://doi.org/10.1097/NEN.0000000000000197>
- Nemerita NS, Ambrus A, Patel H, Gerfen G, Adam-Vizi V, Tretter L, Zhou J, Wang J, Jordan F (2014) Human 2-oxoglutarate dehydrogenase complex E1 component forms a thiamin-derived radical by aerobic oxidation of the enamine intermediate. *J Biol Chem* 289(43):29859–29873. <https://doi.org/10.1074/jbc.M114.591073>
- Palkovits M (1973) Isolated removal of hypothalamic or other brain nuclei of the rat. *Brain Res* 59:449–450
- Park LC, Albers DS, Xu H, Lindsay JG, Beal MF, Gibson GE (2001) Mitochondrial impairment in the cerebellum of the patients with progressive supranuclear palsy. *J Neurosci Res* 66(5):1028–1034
- Sang S, Pan X, Chen Z, Zeng F, Pan S, Liu H, Jin L, Fei G, Wang C, Ren S, Jiao F, Bao W, Zhou W, Guan Y, Zhang Y, Shi H, Wang Y, Yu X, Wang Y, Zhong C (2018) Thiamine diphosphate reduction strongly correlates with brain glucose hypometabolism in Alzheimer's disease, whereas amyloid deposition does not. *Alzheimers Res Ther* 10(1):26. <https://doi.org/10.1186/s13195-018-0354-2>

- Sheu KF, Blass JP (1999) The alpha-ketoglutarate dehydrogenase complex. *Ann N Y Acad Sci* 893:61–78
- Shi Q, Risa O, Sonnewald U, Gibson GE (2009) Mild reduction in the activity of the alpha-ketoglutarate dehydrogenase complex elevates GABA shunt and glycolysis. *J Neurochem* 109(Suppl 1):214–221
- Sonnewald U, Schousboe A (2016) Introduction to the glutamate-glutamine cycle. *Adv Neurobiol* 13:1–7. [https://doi.org/10.1007/978-3-319-45096-4\\_1](https://doi.org/10.1007/978-3-319-45096-4_1)
- Starkov AA (2013) An update on the role of mitochondrial alpha-ketoglutarate dehydrogenase in oxidative stress. *Mol Cell Neurosci* 55:13–16. <https://doi.org/10.1016/j.mcn.2012.07.005>
- Starkov AA, Fiskum G, Chinopoulos C, Lorenzo BJ, Browne SE, Patel MS, Beal MF (2004) Mitochondrial alpha-ketoglutarate dehydrogenase complex generates reactive oxygen species. *J Neurosci* 24(36):7779–7788
- Sunkin SM, Ng L, Lau C, Dolbear T, Gilbert TL, Thompson CL, Hawrylycz M, Dang C (2013) Allen Brain Atlas: an integrated spatio-temporal portal for exploring the central nervous system. *Nucleic Acids Res* 41:D996–D1008. <https://doi.org/10.1093/nar/gks1042>
- Supplie LM, Duking T, Campbell G, Diaz F, Moraes CT, Gotz M, Hamprecht B, Boretius S, Mahad D, Nave KA (2017) Respiration-deficient astrocytes survive as glycolytic cells in vivo. *J Neurosci* 37(16):4231–4242. <https://doi.org/10.1523/JNEUROSCI.0756-16.2017>
- Terwel D, Bothmer J, Wolf E, Meng F, Jolles J (1998) Affected enzyme activities in Alzheimer's disease are sensitive to antemortem hypoxia. *J Neurol Sci* 161(1):47–56
- Thevenet J, De Marchi U, Domingo JS, Christinat N, Bultot L, Lefebvre G, Sakamoto K, Descombes P, Masoodi M, Wiederkehr A (2016) Medium-chain fatty acids inhibit mitochondrial metabolism in astrocytes promoting astrocyte-neuron lactate and ketone body shuttle systems. *FASEB J* 30(5):1913–1926. <https://doi.org/10.1096/fj.201500182>
- Tretter L, Adam-Vizi V (2004) Generation of reactive oxygen species in the reaction catalyzed by alpha-ketoglutarate dehydrogenase. *J Neurosci* 24(36):7771–7778
- Uhlen M, Fagerberg L, Hallstrom BM, Lindskog C, Oksvold P, Mardinoglu A, Sivertsson A, Kampf C, Sjostedt E, Asplund A, Olsson I, Edlund K, Lundberg E, Navani S, Szgyarto CA, Odeberg J, Djureinovic D, Takanen JO, Hober S, Alm T, Edqvist PH, Berling H, Tegel H, Mulder J, Rockberg J, Nilsson P, Schwenk JM, Hamsten M, Feilitzten K, Forsberg M, Persson L, Johansson F, Zwahlen M, Heijne G, Nielsen J, Ponten F (2015) Proteomics. Tissue-based map of the human proteome. *Science* 347(6220):1260419. <https://doi.org/10.1126/science.1260419>
- Waagepetersen HS, Hansen GH, Fenger K, Lindsay JG, Gibson G, Schousboe A (2006) Cellular mitochondrial heterogeneity in cultured astrocytes as demonstrated by immunogold labeling of alpha-ketoglutarate dehydrogenase. *Glia* 53(2):225–231. <https://doi.org/10.1002/glia.20276>
- Wagner GR, Payne RM (2013) Widespread and enzyme-independent Nepsilon-acetylation and Nepsilon-succinylation of proteins in the chemical conditions of the mitochondrial matrix. *J Biol Chem* 288(40):29036–29045
- Wang Y, Guo YR, Liu K, Yin Z, Liu R, Xia Y, Tan L, Yang P, Lee JH, Li XJ, Hawke D, Zheng Y, Qian X, Lyu J, He J, Xing D, Tao YJ, Lu Z (2017) KAT2A coupled with the alpha-KGDH complex acts as a histone H3 succinyltransferase. *Nature* 552(7684):273–277. <https://doi.org/10.1038/nature25003>
- Weinert BT, Scholz C, Wagner SA, Iesmantavicius V, Su D, Daniel JA, Choudhary C (2013) Lysine succinylation is a frequently occurring modification in prokaryotes and eukaryotes and extensively overlaps with acetylation. *Cell Rep* 4(4):842–851
- Zhang Z, Tan M, Xie Z, Dai L, Chen Y, Zhao Y (2011) Identification of lysine succinylation as a new post-translational modification. *Nat Chem Biol* 7(1):58–63. <https://doi.org/10.1038/nchembio.495>
- Zhang Y, Wang G, Song L, Mu P, Wang S, Liang W, Lin Q (2017) Global analysis of protein lysine succinylation profiles in common wheat. *BMC Genom* 18(1):309. <https://doi.org/10.1186/s12864-017-3698-2>

**Publisher's Note** Springer Nature remains neutral with regard to jurisdictional claims in published maps and institutional affiliations.